Spring 2023

Development of a Regeneratively Cooled Liquid Rocket Engine

Dillon Petty
The University of Akron, dmp150@uakron.edu

Nicole Zimmerli
The University of Akron, ngz2@uakron.edu

DEVELOPMENT OF A REGENERATIVELY COOLED LIQUID ROCKET ENGINE

By:

Dillon Petty

Nicole Zimmerli

UA Advisor: Dr. Manigandan Kannan

Final Report for MECE:497 Senior/Honors Design, Spring 2023

Department of Mechanical Engineering

College of Engineering and Polymer Science

Faculty Advisor: Dr. Manigandan Kannan

Faculty/Honors Advisor: Dr. Dane Quinn

Faculty/Honors Reader 1: Thomas Teasley

Faculty/Honors Reader 2: Dr. Guo-Xiang Wang

Abstract

An additively manufactured (AM) liquid rocket engine, consisting of injector, combustion chamber, and nozzle, was designed and printed using state of the art methods and materials. The parts were manufactured using laser powder bed fusion. Additive manufacturing allowed for complex geometries and features, such as printing manifolds onto the components with a reduced number of parts. Additive, regenerative cooling channels were designed into the chamber and nozzle to allow for long duration steady-state operation.

The feed system for the engine was designed and built to allow for pressure-regulated and steady-state testing. Tanks for the fuel and oxidizer were designed and built for a maximum 15 second test duration. A purging system was developed to keep the propellant lines clean and aid in engine shutdowns. A testing campaign was designed and conducted for characterization of this engine, including proof, water flow, cold flow, and hot fire testing. Issues with ignition were experienced and ultimately three hot fire tests were achieved for a total duration of ~14.5 seconds. This project shows that additive manufacturing can simplify many of the complicated and expensive operations when designing and building a liquid rocket engine, lowering the barrier to entry to the space industry.

Table of Contents

List of Figures

List of Tables

Nomenclature

A = area
C_d = discharge coefficient
C_f = thrust coefficient
C^* = characteristic velocity
D = tank diameter
d = clearance hole diameter
E = edge distance from hole
F = force
h = specific enthalpy
L^* = characteristic length
$\dot{m}$ = mass flow rate
N = number of bolts
P = pressure
s = specific entropy
t = time
V = volume

Subscripts

1 = upstream of the injector
2 = downstream of the injector
b = bolt
c = chamber
i = injector
t = throat
v = vapor

Symbols

Δ = delta across injector
ρ = density
σ = stress

1. Introduction and Objectives

A liquid rocket engine (LRE) is a combustion device that uses liquid and/or gaseous propellants to generate the thrust needed to launch a rocket. The most common type is a bipropellant LRE, which uses two chemicals: a fuel and an oxidizer. Each propellant is stored separately in a tank, and when the engine turns on, the high-pressure fluids flow through tubing and valves towards the injector. The injector mixes the two as they enter the combustion chamber, where they are ignited. The combustion gases then flow through a nozzle, which generates the thrust needed to lift a launch vehicle. This capstone project aimed to design, manufacture, and test a regeneratively cooled liquid rocket engine. The motivation behind this project was to dramatically transform the propulsion capabilities of the university's Akronauts Rocket Design Team by utilizing state-of-the-art technology and manufacturing processes.

The Akronauts Rocket Design Team is a student-led organization that gives members the opportunity to gain experience and skills in the intercollegiate rocketry setting. For propulsion, the team has almost entirely used solid propellants in the past. Solid propellants are relatively simpler compared to liquids, and the large community of amateur rocketry almost exclusively uses solid propellants. For example, solid rocket motors of various sizes can be purchased commercially and flown in a rocket, but no such solution exists for liquids. The complexity of developing a LRE and the resources involved make it attainable for only a handful of universities across the country. The Akronauts liquid propulsion program has been running for approximately two years and, as of September 2022, has successfully tested their first liquid rocket engine, making the University of Akron the first university in the state of Ohio to do so. An image of the Akronauts' first hot fire test can be seen in Figure 1.

Figure 1. Akronauts hot fire test in September 2022.

Liquid propulsion has many advantages over solid propulsion, including reusability, more control (it can be throttled and turned off), higher specific impulse, and longer burn times. For these reasons they are the preferred option in the aerospace industry. The same reasons led the Akronauts to start developing liquid propulsion, but the first design of an ablative engine showed itself to be limiting: it is not fully reusable and has burn times between 5-10 seconds. This project focused on eliminating such limitations by implementing regenerative cooling, resulting in a fully reusable engine and burn times limited only by the size of the propellant tanks.

To properly test a regeneratively cooled LRE, a thrust chamber assembly (TCA), which consists of an injector, combustion chamber, and nozzle, needed to be designed. Additionally, a feed system, including tanks, propellant lines, and nitrogen external pressurant system needed to be designed and added to the existing test stand. This project was able to utilize the Akronauts Rocket Design Team's test stand for hot fire testing, but the controls systems still needed to be upgraded. In order to achieve thermal steady state, the system was designed for testing durations up to 15 seconds.

2. Engine Design

The test article, named HORNET (High-Altitude Sub-Orbital Regeneratively-Cooled Nitrous Ethanol Thruster), is an additively manufactured, regeneratively cooled, bipropellant liquid rocket engine. As the name suggests, it uses nitrous oxide and ethanol as propellants, and is designed to a nominal operating condition of 400 psia chamber pressure and a mixture ratio (MR) of 3.2. The engine is designed to output 800 lbf of thrust at sea level. The engine was manufactured using state-of-the art additive manufacturing (AM) capabilities. Both the injector and combustion chamber for this engine were printed from GRCop-42 using laser powder bed fusion (L-PBF). The engine hardware was printed at NASA's Marshall Space Flight Center,

which has sponsored the project. Figure 2 below shows a rendering of the design and the printed assembly.

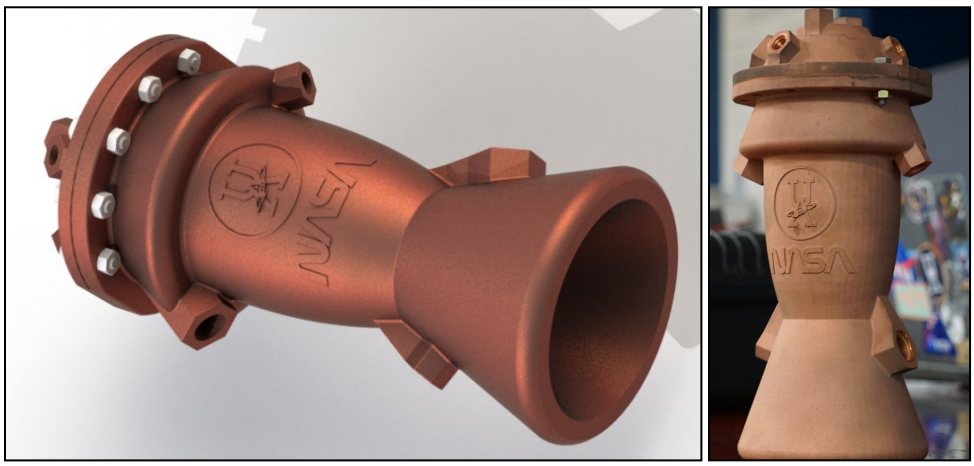

Figure 2. Rendering of the HORNET engine assembly (left) and finished assembly (right).

2.1. Additive Manufacturing

Additive manufacturing has grown dramatically in the aerospace industry in recent years, especially for propulsion applications. There are several advantages to AM over traditional manufacturing for propulsion, most notably reducing lead times by factors between 2-10 and cost by more than 50% [1]. Other advantages include lightweighting of structural components, significantly reducing part counts, and the ability to print complex geometry and internal features [2]. The latter is particularly advantageous when used with heat transfer devices as newly high-performance designs can be made that were not possible or cost-effective with traditional manufacturing.

By utilizing the power of additive manufacturing cooling, channels were printed directly into the combustion chamber thus significantly simplifying an otherwise complicated manufacturing process. Additionally, fluid manifolds were printed onto the main components for the fuel inlet and exits of the chamber, and for fuel and oxidizer inlets of the injector. The manifolds direct the flow to and from the coolant channels, as well as distribute the propellants to the injector orifices. Such features not only reduced weight and part count, but also reduced any need of welding on manifolds post printing. Lastly, AM allowed the nozzle and combustion chamber to be printed as one part, further simplifying the assembly.

2.1.1. Laser Powder Bed Fusion and Post Processing

There are several AM methods, but the printing method chosen was laser powder bed fusion. L-PBF, also known as selective laser melting (SLM), uses a laser to weld metal powder together layer by layer until the final component is created. This process has been matured to produce high performing combustion devices and is advantageous for its high feature resolution compared to other additive processes [1]. This method uses a sealed, inert printing environment

which results in the main disadvantage of limited build volume, but this was not an issue for the thruster class engine. Figure 3 below shows a graphic of a L-PBF printer and the key components involved.

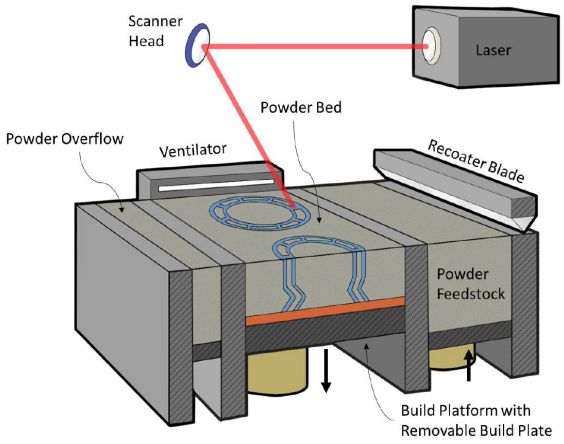

Figure 3. Laser powder bed fusion setup. [1]

As with all additive manufacturing methods, post processing was required before the part could be tested. The key post processing steps for the chamber and injector were powder and build-plate removal, heat treatment, and machining. Figure 3 shows a typical L-PBF printer setup and the various components involved. When a part is finished printing, it is completely buried in powder. This powder needs to be removed from the external and internal surfaces. It is important that it happens prior to heat treatment as the residual powder can sinter together within voids, causing blockages [3]. The heat treatment used was Hot Isostatic Pressing (HIP). This process is used to reduce porosity in the parts, achieving higher densities closer to the wrought material [4]. In addition, the HIP process can also act as a stress relief to reduce residual stresses from the printing process. Lastly, machining is done on all the sealing surfaces and ports to reduce the surface roughness that results from the printing process. Following this, the post processing stage ends, and the part can begin assembly and testing. The process flow for the combustion chamber designed in this project is shown below in Figure 4 and highlights some of the key post processing steps.

2.1.2. Computer Topography (CT) Scanning

Non-destructive evaluation (NDE) methods are an additional post processing step used to verify a part is within the design tolerances and ready to be used. Computer topography (CT) scanning is an NDE method that uses x-rays to inspect a part for trapped powder, cracks, foreign object debris (FOD), and other features that are not visible from outside the part. Since both ends of the coolant channels were inside manifolds, flow testing alone could not verify that all channels were free of powder. Powder presence can lead to flow restriction or blockage, resulting in chamber hot-wall failure. Then, CT scanning was performed on the combustion

chamber at MSFC to look for trapped powder within the cooling channels. The scan showed that the chamber was free of powder, evidenced by the third image shown in Figure 4 below.

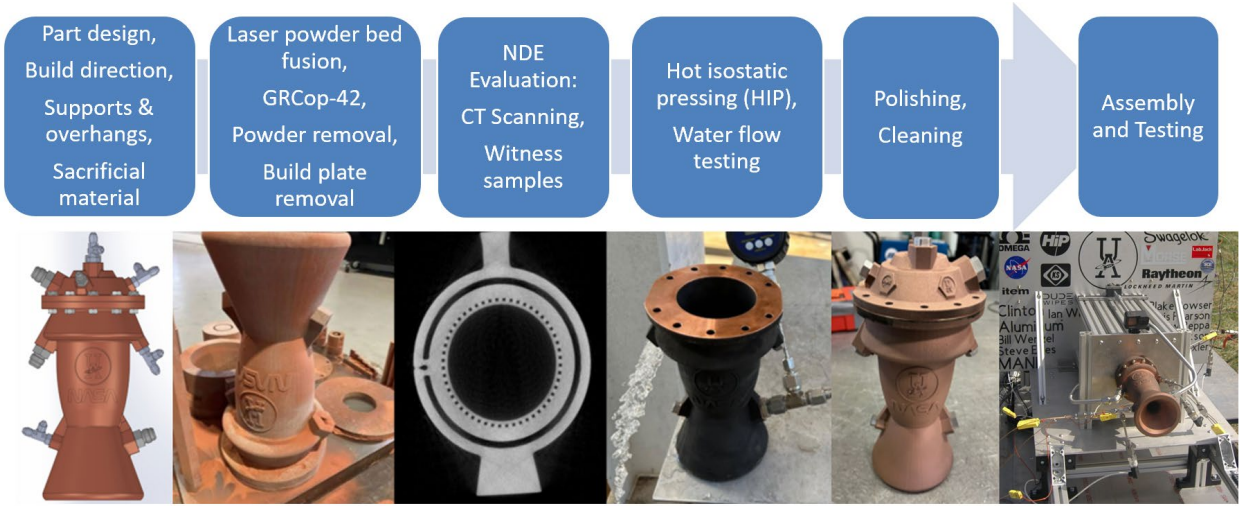

Figure 4. Additive manufacturing process flow and key considerations.

2.2. Combustion Chamber Design

The material chosen for this was GRCop-42, a copper, chromium, and niobium alloy (Cu-4 at.% Cr-2 at.% Nb). GRCop-42 is a dispersion strengthened alloy with high conductivity and high strength at extreme operating temperatures, which can reach upwards of 1400 °F for sustained durations (depending on strength and creep requirements). This, in addition to oxidation resistance, established powder supply chain, and substantial property development made GRCop-42 the preferred material for the combustion chamber and injector [4].

The chamber pressure design was designed to operate at the same chamber pressure as the previous engine, 400 psia, but at an increased thrust of 800 lbf. Using NASA's Chemical Equilibrium Applications (CEA) software, several performance characteristics were calculated at the exit of an ideally expanded nozzle. For the combustion chamber design, the two key outputs of CEA were characteristic velocity (c*) and the thrust Coefficient (C_f). Using the thrust coefficient, expected chamber pressure (P_1), and desired thrust (F), the below equation was used to calculate the throat area of the engine.

$$A_t = \frac{F}{P_1 C_f} \tag{2.1}$$

The chamber diameter was kept the same as the previous VENM 4 chamber because it was desired to standard the injector face diameter with the previous engine. The resulting subsonic area ratio was sufficient for avoiding flow losses. Common ratios are between 2-5 [5]. Using the throat area and characteristic velocity from CEA, the required total mass flow rate was calculated using the Equation 2.2. This result, in addition to the target mixture ratio, is then used to

determine the flow rate of fuel and oxidizer. These flow rates are also used later in injector sizing calculations.

$$\dot{m} = \frac{p_1 A_t}{c^*} \tag{2.2}$$

The length of the barrel section of the chamber was determined by designing to a recommended characteristic length (L*) of 30-120 inches [6]. To account for the significant chamber radii, the chamber volume (V_c) was approximated by calculating the volume of the frustrum of a cone at various points and summing the results. The characteristic length of the engine was designed to be 33 inches to reduce part length and weight, as well as print costs.

$$L^* = \frac{V_c}{A_t} \tag{2.3}$$

2.2.1. Coolant Channel Design

The combustion chamber coolant channels were designed using the Bartz heat transfer correlations to generate the coolant temperatures. The engine used rectangular channels and the width and height were varied to minimize pressure drop and have a near-linear coolant temperature increase. The predicted heat flux was based on previous testing data scaled using the Bartz equation [5]. It was scaled based on chamber pressure, characteristic velocity, and chamber geometry. The output temperatures were normalized based on the highest expected wall temperature and are shown below in Figure 5.

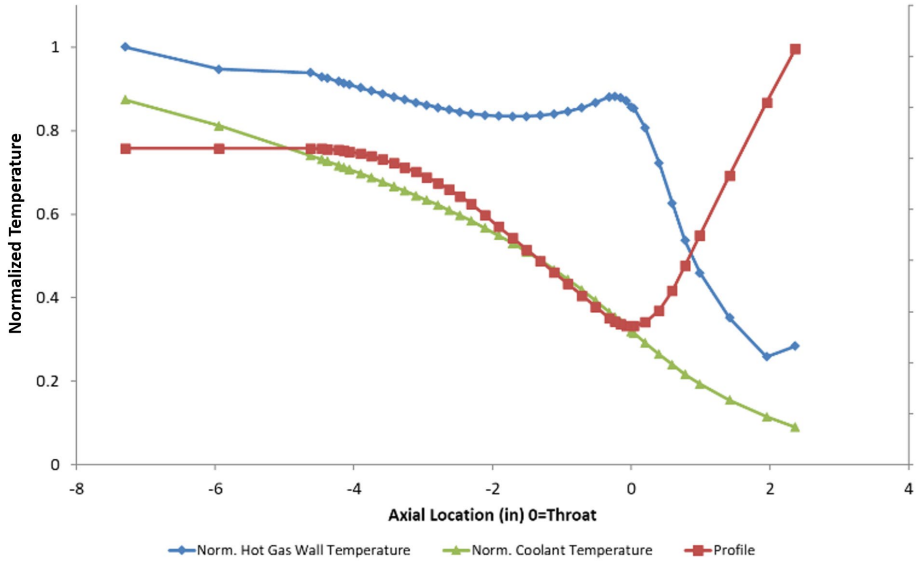

Figure 5. Coolant output temperatures (normalized).

2.3. Nozzle Design

The nozzle was designed to be regeneratively cooled and printed as the same part of the combustion chamber. The nozzle was designed to be slightly overexpanded at sea level to improve the performance at higher altitudes that it would see during a flight. The required expansion area ratio, or the ratio of the exit area to the throat area, was found by running a NASA CEA analysis with a defined pressure ratio (P_e/P_c). The contour geometry is a traditional bell-curve nozzle that was designed using the Method of Characteristics [7] to obtain a minimum length nozzle. The nozzle geometry was slightly truncated to reduce nozzle weight and manufacturing costs. By using additive manufacturing, it was possible to create a more efficient nozzle compared to the conical graphite nozzle produced for the VENM 4 engine.

2.4. Injector Design

The injector was designed to be produced using additive manufacturing, which allowed for complex and lightweight manifolds and ports printed with the injector as one piece. All the fluid inlets and sensor taps for pressure and temperature measurements used a printed port that was machined in the part's post-processing. One design consideration was to make the flange and bolting pattern the same as used for the previous injector created for VENM 4 engine, allowing the possibility of matching the chamber with a traditionally machined injector if desired. A key design constraint for using AM was keeping the overhang angles 30° or less to avoid needing support structures. Additionally, the injector was printed face down, requiring it to be separated from the built plate using wire electrical discharge machining (EDM). Figure 6 below shows the injector before and after the HIP treatment.

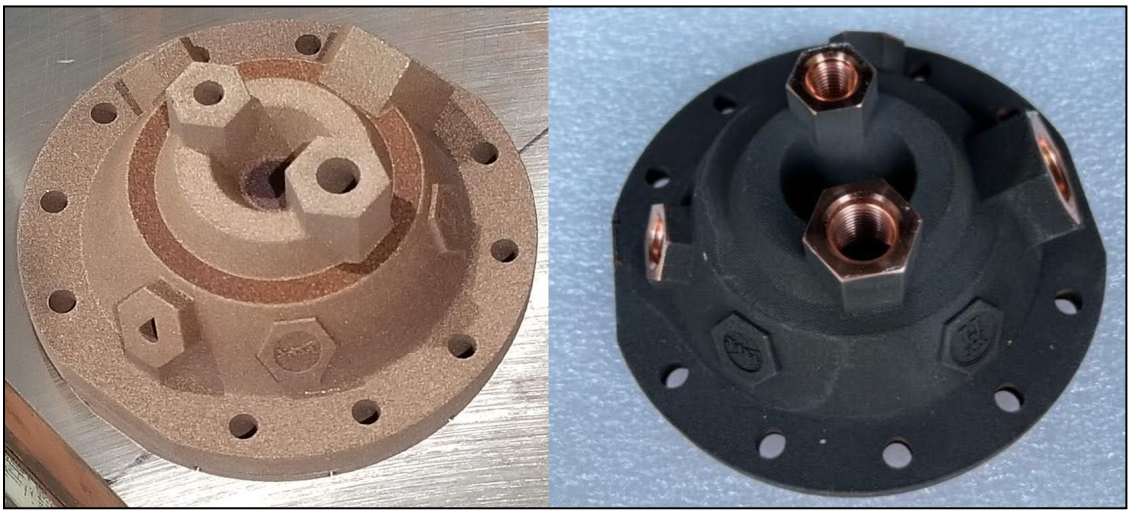

Figure 6. The HORNET injector on the build plate (left) and after HIP (right).

The injector uses an F-O-F impinging triplet injector scheme with 12 elements. This element scheme was chosen due to the experience of the authors and Akronauts Rocket Design Team with previous injectors. The orifice flow area on the ethanol side was designed using the single

phase incompressible (SPI) model shown in Equation 2.4. The nitrous oxide flow area was designed using the Dyer model, also known as the Non-Equilibrium Non-Homogenous (NHNE) model since the chamber pressure falls below the vapor pressure of nitrous oxide. These conditions have been seen both in literature and in the authors' testing experience to result in vapor formation within the injector orifices, and the phenomenon has been studied to create and validate the Dyer model [8].

$$\dot{m}_{SPI} = A_i C_d \sqrt{2\rho_1 \Delta P} \tag{2.4}$$

The injector was designed with a minimum stiffness, also known as the ratio of pressure drop to chamber pressure, of 20% to avoid having combustion instabilities. For steady state densities, the stiffness was designed to be 60% to allow for a wide variety of flowrates. Since the fuel density is lower during startup than at steady state, the stiffness drops to around 21% until the ethanol heats up. Also, compared to machined orifices, a lower discharge coefficient needs to be assumed during the design to account for the surface roughness from L-PBF and shrinkage that can occur during printing.

2.5. Igniter

The igniter for this engine is a small grain of ammonium perchlorate composite propellant (APCP) mixed with titanium to produce hot white sparks. The grain is suspended along the center axis of the thrust chamber using a 3D printed piece and is remotely ignited using an electric match. After the engine ignites, the igniter assembly is blown out of the engine. This ignition method was chosen for its simplicity and success in igniting the team's previous nitrous/ethanol engine. The grain was designed to be small enough to easily pass through the throat of the engine, and so that the flames and sparks generated were directed outwards towards the impingement points of the injector. This igniter was tested previously to determine how long it takes for the flame and sparks to fully establish, which was used to delay the propellant flow to prevent blowing out the igniter. Figure 7 shows an image of the igniter during this burn test, which also shows the sparks and flame formed from it. Even though this ignition style proved successful for the team's previous nitrous/ethanol engine, it did not have the same success for the regeneratively cooled engine and is discussed in section 5.7. Ignition Discussion.

Figure 7. Burn test of an APCP igniter (left) and modified igniter and holder (right).

3. Test Stand Design

The test stand used for the HORNET engine was constructed by modifying the pre-existing test stand the University of Akron Akronauts Rocket Design Team previously built. A new mounting plate was designed to attach the HORNET thrust chamber to the stand. Additionally, an external pressurant and purge system, larger tanks, and upgraded controls and data acquisition systems were added to the stand.

3.1. Feed System

The feed system of the test stand carries the fuel and oxidizer from the tanks to the thrust chamber assembly. The feed system is pressure-fed and uses gaseous nitrogen to regulate the pressure in the tanks. The regulated tank pressure allows for steady state flow rates and operating conditions. Cavitating venturi flowmeters are used to control the mass flow rate of the propellants to achieve the ideal mixture ratio (MR), or oxidizer/fuel ratio, in the thrust chamber. These were used because venturis can set the mass flow rate given only an inlet pressure and inlet density, regardless of downstream pressure. The system will have the same mass flowrate at startup, when the downstream pressure is ambient, and when there is full chamber pressure. The only requirement for this method is that the venturi is cavitated, which is determined by the pressure ratio. The pressure ratio is defined by the downstream pressure divided by the upstream pressure. To be cavitated, the pressure ratio should be equal to or less than 0.80 [9–11]. Under this condition, the flow rate can be calculated using the Equation 3.1 below. This equation is a modification of Equation 2.1 and still assumes a single phase and incompressible fluid. The main difference is the venturi version uses the fluid's vapor pressure instead of the downstream pressure.

$$\dot{m}_{venturi} = A_t C_d \sqrt{2\rho_1 (P_1 - P_v)} \tag{3.1}$$

In addition to the venturis, mass flow rate is measured by load cells placed underneath the propellant tanks that measure weight during testing. The slope of the tank weight vs. time curve gives the net mass flow rate out of the tank. For the load cells to properly measure the weight of the tanks, a slider system allows for one degree of freedom (DOF) in the vertical direction while still securing the tank to the stand. One source of error from this method is the reaction forces caused by the tanks' fluid connections. To minimize these, stainless steel flexible hoses are used to connect the tanks to the rest of the system. Hard tubing was used but intentional bends were included to allow the end of the tube to deflect with little reaction forces.

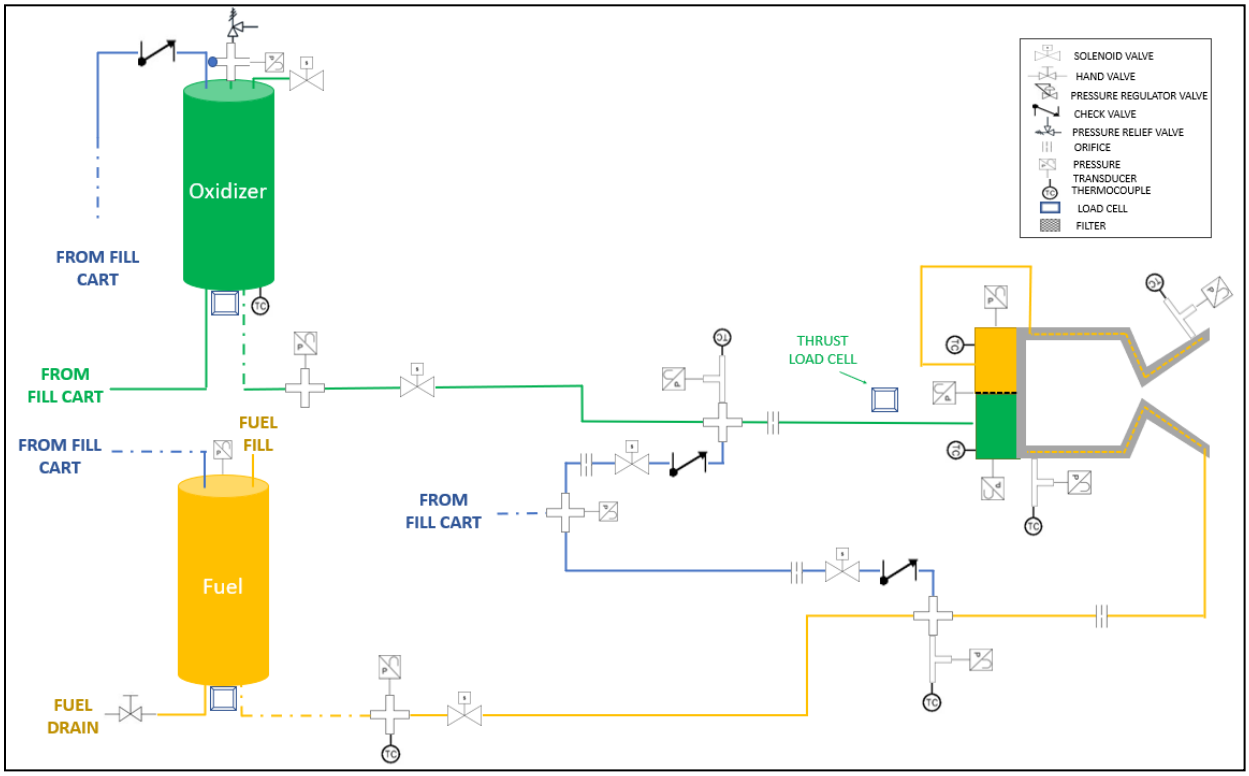

Figure 8. P&ID of the HORNET feed system.

Figure 8 shows the piping and instrumentation diagram (P&ID) of the current test stand configuration. The green lines show the path of the oxidizer, the yellow shows the path of the fuel, and the blue shows the path of the external pressurant. The length and shape of the connecting lines is not to scale.

Solenoid valves are located on each feed line to remotely control the flow of propellant to the injector. These valves are normally closed so that if the test stand loses power during a test, the valves will automatically close, causing the engine to shut down. Pressure transducers and thermocouples are located at multiple locations across the feed system to measure the pressure and temperature to calculate propellant density and enthalpy.

3.2. External Pressurant & Purge System

The external pressurant and purge system (EPPS) is used to pressurize the tanks and move the propellants through the system. The two most common inert gases used for this application in industry are helium and nitrogen. Helium is lighter, resulting in higher performance, and is required in certain applications such when using liquid hydrogen. However, it is also much more expensive than nitrogen, and for a test stand where weight is not the main concern, nitrogen was chosen to be the pressurant for the system. The nitrogen purge system connects to each propellant line right after the solenoid valve, so that everything after the valve gets removed after a test is completed. Each purge line has a check valve to keep propellant and/or combustion gases out of the nitrogen system. Nitrogen flow is also controlled with solenoids and the flow rate is metered by an orifice.

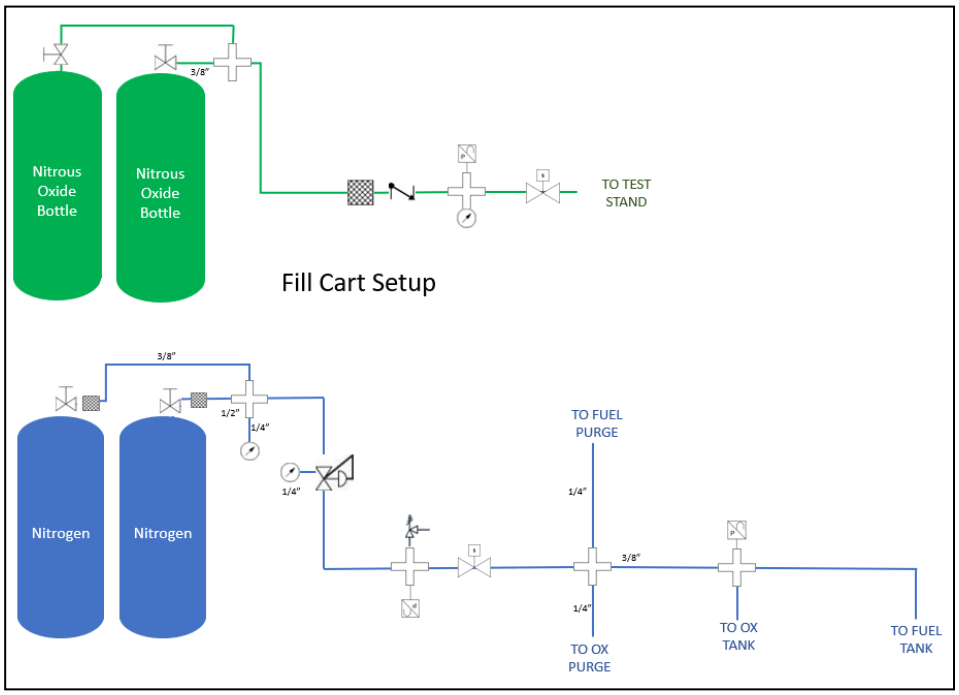

Figure 9. P&ID of the External Pressurant and Purge System.

The EPPS, along with the nitrous fill system, is housed on a separate fill cart that attaches to the test stand through multiple hoses. The fill cart assembly can be seen in Figure 10. The fill cart can be seen holding two bottles: the left is nitrogen, and the right is nitrous oxide. For testing, an additional bottle of each were connected and chained to the cart to prevent needing to replace the bottles as often. The design uses a single pressure-reducing regulator to regulate the 4500 psi nitrogen bottles down to the operating pressures. Given that there is only one pressure regulator, the fuel tank pressure, oxidizer tank pressure, and purge inlet pressure are all coupled. Figure 9 shows the P&ID for the system and how each of the outlets are connected to the same source. The addition of a second regulator would give the test stand much more flexibility to quickly test different mixture ratios as the tank pressures could be set independently. An

alternative solution is adding orifices to meter the flow rate to each outlet, but this control was not an initial requirement for the system.

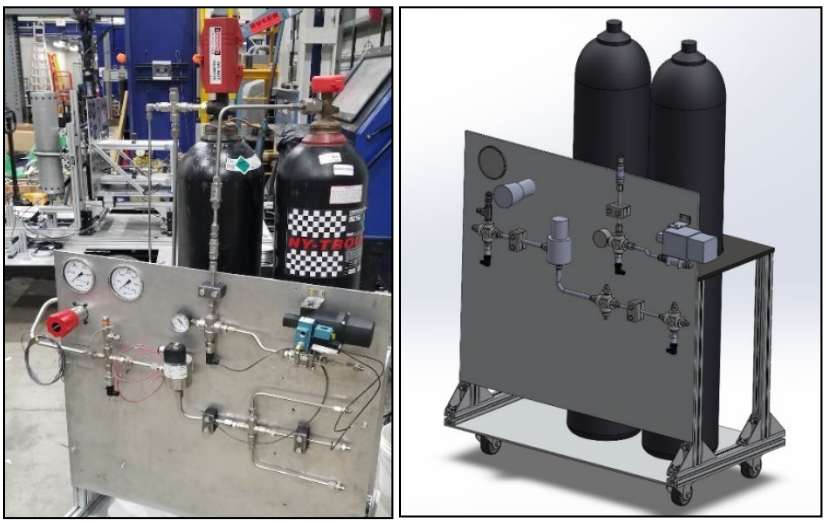

Figure 10. Fill cart assembly (left) and CAD (right).

The EPPS design includes a pressure relief valve (PRV) to protect the system in the case of a regulator failure. The pressure relief valve opens at a set pressure to relieve pressure from the feed system so that it does not over-pressurize components, most notably the nitrogen main valve. Over-pressurization of the nitrogen main valve could result in one of two failures: most likely it would fail closed, and the stand would not be able to be pressurized. If it failed open, the tanks and feed system would unintentionally be pressurized, posing an extreme safety risk. All tubing and fittings were selected to be rated to a minimum of 3,000 psi, and the PRV was set to 2,400 psi.

When testing, it was necessary to make sure there was enough nitrogen to properly fill the volume of the fuel and oxidizer tanks during testing while staying above the regulator set pressure. To determine this, the ideal gas law was used and simplified by assuming isothermal expansion of the nitrogen gas. This can be seen in Equation 3.2 below. State 1 represents the volume of the two nitrogen bottles and initial pressure in them. State 2 represents the bottle volume plus the volume of both the fuel and oxidizer tank. Using these, the ending pressure was able to be calculated to determine if the pressure could be regulated or not.

$$P_2 = \frac{P_1 V_1}{V_2} \tag{3.2}$$

3.3. Thrust Measurement System

The test stand has a thrust measurement system so that the engine performance can be measured. This is achieved by using a sled that can slide in the horizontal direction, keeping a

DOF to measure the thrust output of the engine. The sled includes the thrust chamber mounting plate, as well as a blast plate to protect the stand in the case of a chamber failure. All valves for the propellant and purge lines are mounted to the blast plate, on the opposite side of the TCA, as seen in Figure 11. Just like the tank weight load cells, stainless steel flexible tubing is used to connect to the tanks to minimize reaction forces and measurement errors.

Figure 11. Test stand CAD model (left), cage assembly (middle), and blast plate (right).

3.4. Propellant Tank Design

There are two tanks on the test stand, one for nitrous oxide and one for ethanol. The tanks were designed to be able to hold enough propellant volume for a 15-second burn time and to have a factor of safety (F.S.) of 2.0 at the proof pressure. The proof pressure targeted during hydrostatic testing was 2400 psi. This number is 1.5x higher than the maximum expected operating pressure (MEOP) that the tanks will see, which was originally 1600 psi. However, during the waterflow testing, mentioned in section 4.2. Water Flows, the 1600 psi tank pressure was determined to be too low of a set pressure for the tanks because of the pressure drop through the nitrogen lines. The final set pressure for the tanks was 2000 psi. The team determined that the tanks were still rated for the new expected pressures due to the conservative F.S. at the proof pressure and successful hydrostatic test at 2400 psi.

Due to the long combustion time of 15 seconds, the oxidizer tank was designed to be 72 inches, and the fuel tank was 20 inches. The difference in length is due to the density of the fluids and the 3.2:1 mixture ratio between the nitrous oxide and ethanol. However, between water tests, cold flows, and hot fire tests, the desired test duration could be anywhere from 5 seconds to 15 seconds. Following a test, all remaining nitrous oxide and nitrogen in the tanks had to be vented. To avoid wasting propellant during shorter tests, the oxidizer tank's length was designed to be adjustable by using modules. The ends of the tanks are sealed by bulkheads, and couplers were designed to fit in between sections of tube stock when using more than one module. Using this method, the oxidizer tank can be 24 in, 48 in, or 72 in long. Additionally, each connection was sealed with two O-rings for redundancy.

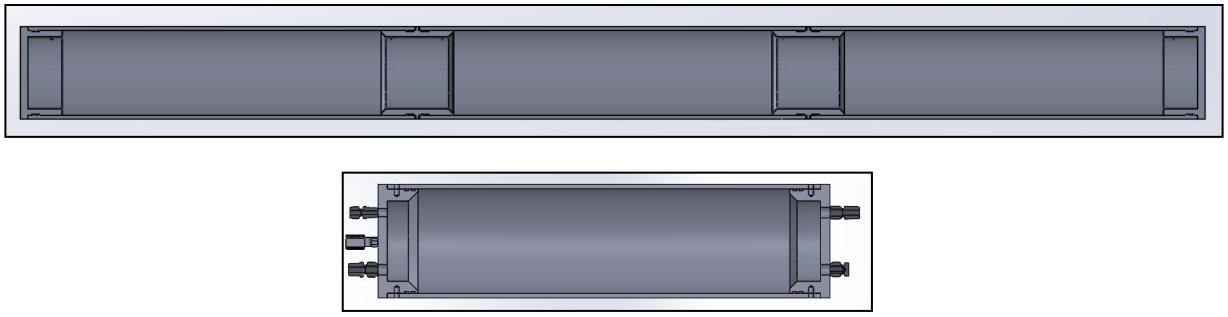

Figure 12. CAD of the oxidizer tank (top) and fuel tank (bottom).

The oxidizer tank holds two valves, a pressure relief valve that actuates when the pressure goes beyond a set value of 2,200 psi and a vent valve. The vent valve serves to empty the tank at the end of the test, as well as reduce pressure to allow for filling of more nitrous oxide. The vent is also connected to a dip-tube within the tank to ensure a portion of the tank is kept empty for ullage. This is mainly for safety. Since the tank will be completely sealed post-filling, a small percentage of the tank volume should be deliberately left free of liquid to allow for liquid nitrous expansion with the ensuing increase of temperature as the tank sits idle before a test [12]. A passive vent is also present on the tank and is a small orifice fitting that allows the tank to slowly depressurize over time. This is a fail-safe put in place to allow the tank to depressurize if the power is cut to the stand. It is unsafe to have a person next to the test stand while nitrous oxide is loaded, so the passive vent valve allows the tank to slowly depressurize without a person needing to go to the stand to manually fix something.

Both tanks are connected to the EPPS to allow for pressurization during testing. The EPPS line that connects to the oxidizer tank has a check valve on it. This prevents the nitrous oxide vapor from back-flowing through the pressurant line and potentially mixing with ethanol in the fuel tank. As mentioned before, the fuel and oxidizer tank are connected to the same nitrogen inlet. A check valve was included on the oxidizer nitrogen line to prevent the self-pressurized nitrous oxide from entering the nitrogen system and fuel tank.

3.4.1. Filling and Draining Procedures

The fuel tank is relatively easy to fill. Ethanol is easy to handle because it is a mild, non-hazardous, and non-toxic chemical. Ethanol is procured through gallon jugs and is filled by directly pouring the jugs into the fuel tank using a funnel. After testing, the remaining ethanol is drained into a jug by opening a hand valve on the bottom of the fuel tank. This happens after the nitrogen and nitrous oxide have been vented and the stand is safe to approach.

Due to nitrous oxide being a saturated liquid-vapor mixture at room temperature, the fill procedure for the oxidizer tank takes a bit longer than the ethanol fill. It is required that no personnel be near the lines or test stand during the oxidizer fill procedure, as oxidizer is extremely flammable and thus creates a safety risk. The oxidizer tank is filled by using a difference in pressure from the nitrous oxide cylinder and the oxidizer tank. The cylinder is

supplied at around 500 psi, but this exact pressure fluctuates ± 50 psi depending on the temperature of the cylinder. The pressure will change once the cylinder is opened and the nitrous oxide expands. The oxidizer tank has a vent valve attached as previously mentioned in section 3.4. Propellant Tank Design. This vent valve is open during the entire fill procedure to lower the pressure in the oxidizer tank relative to the cylinder. Because the pressure is nearly equal between the fill cylinder and the oxidizer tank, the valve between them needs to be closed periodically throughout the fill procedure. This allows the tank to vent off excess vapor pressure and create a larger difference in pressure from the cylinder to the tank.

3.4.2. Tank Stress Analysis

Structural considerations of the pressure vessel design included bolt shear stress, tube tensile stress, bearing stress on bolt clearance holes, and tube shear stress as referred to as bolt tear-out stress [13]. The critical failure mode for this design was the bolt tear-out stress and is calculated using Eqs. (3.1) – (3.2). In these equations, $D_{i,tube}$ is the inner diameter of the tank tube, N is the number of bolts, F_b is the force on each bolt, t is the thickness of the tank tube, d is the bolt clearance hole diameter, and E is the distance between the hole center and end of the tube. Table 1 shows these calculations with the tank design as well as the tank's smallest safety factor.

$$F_b = \frac{\frac{\pi}{4} D_{i,tube}^2 \times P_{MEOP}}{N} \tag{3.2}$$

$$\sigma_{tear-out} = \frac{F_b}{\left(E - \frac{d}{2}\right) \times 2t} \tag{3.3}$$

Table 1. Tank bolt tear-out stress calculation.

Bolt tear-out stress		
Max Operating Pressure	2400	psi
Do, tube	6.00	in
Di, tube	5.54	in
Number of bolts	24	bolts
Force per bolt	2409	lbs
Bolt clearance hole diameter	0.35	in
E, tube shear thickness	0.50	in
Min shear thickness	0.33	in
Tube thickness	0.25	in
Stress, tear out	14826	psi
6061 shear strength	30000	psi
FS, tear-out	**2.02**	

3.5. Data Acquisition and Control Systems

The instrumentation used in the test stand and fill cart are crucial for ensuring not only proper and safe operation but also accurate measurements of performance. The current configuration includes a control box that houses the relays, data acquisition (DAQ) systems, and power supply connections. A LabJack T7 is used as the controller for the system and a LabJack T7 Pro is used as the DAQ. There are multiple sensors throughout the system including E- and K-type

thermocouples, pressure transducers, and load cells. The placement of the instrumentation allows for proper characterization of performance during testing and overall system performance. An image of the layout of the control systems box can be seen in Figure 13.

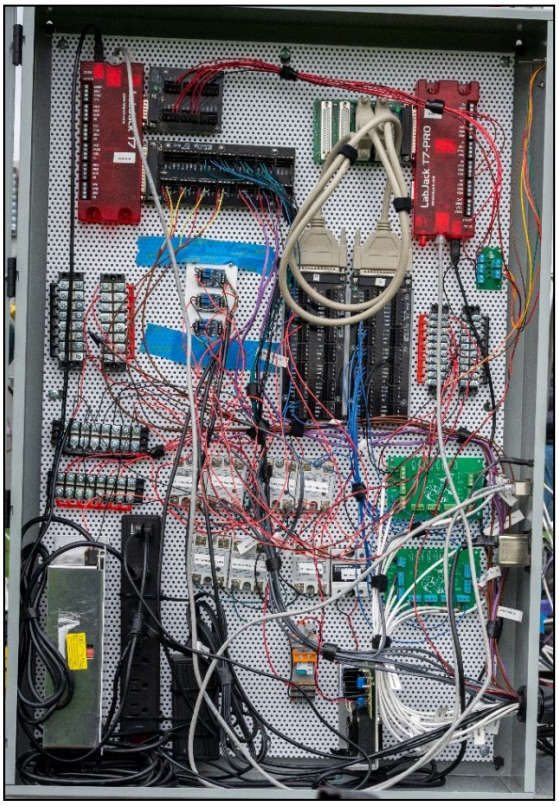

Figure 13. Image of the controls box on the test stand.

A load cell board was designed and added to the controls of the test stand to amplify the load cell outputs to better read the data. A common problem in the past was noisy load cell readings, or a low signal-to-noise ratio. If the difference in weight applied to a load cell only minorly changes the output voltages of the load cell, then the noise will add uncertainty to the true reading. If the output voltage signal is amplified, then that same noise makes a smaller difference in the overall amplitudes of the data.

A custom-written software, called HIVE (HORNET Integrated Vehicle Environment), commands the controller and DAQ from an external computer. HIVE directly relays data to a user interface (UI) for live graph output and saving during testing. HIVE has the capability of reading all the sensors on the test stand and provides a user-friendly interface for various controls such as actuating valves manually, making changes to the timings on the hot fire sequence, actuating warning lights on the stand, and automatically running a shutdown sequence in the instance of an emergency stop. The data is read at 4000 Hz to accurately process data post-testing, since sampling at a higher rate gives a higher accuracy on the signal. Some things happen in fractions of a second, and the data acquisition rate must be high to properly view these

occurrences. The sample rate can be changed in the UI of the HIVE software as well if lower frequency sampling is desired.

4. Testing Methodology

Various component and system-level tests were conducted in characterizing the feed system and the test article. The tests were conducted at the Gas Turbine Testing Facility at the University of Akron with the exception at the hot fire tests, which were conducted at the Northern Ohio Tripoli Rocket Association (NOTRA) launch site in Amherst, OH.

4.1. Hydrostatic Pressure Testing

To verify the feed system can handle the high pressures that are expected during testing, a hydrostatic pressure test is conducted for the whole test stand. The line being tested was first filled with water and uncapped at the end to allow any residual air in the line to escape during the filling process. The line was filled with water as opposed to a compressible gas to reduce the amount of energy being held in the system during the testing process. This way, if there is a failure it will be non-catastrophic, and the system will immediately lose pressure. A hydrostatic pump was then used to slowly bring the line up to the tested pressure. This was done in 500 psi increments until around 1500 psi, in which the pressure in the line was increased in 200 psi increments. A complete list of the tested pressures vs the lines tested is shown in Table 2.

Table 2. Test stand subsystem vs. proof pressure.

Subsystem	Pressure (psi)
Test stand feed system	2,500
Tanks	2,500
N_2O fill cart	1,500
Fill cart before regulator	5,000
Fill cart after regulator	2,500
Combustion chamber	1,200

The pressure tested was determined based off the MEOP to be seen in the various lines. For example, the nitrogen cylinders come at 4500 psi when fully filled, so the lines between the pressure regulator valve and the cylinder were tested to 5000 psi. There are two pressure relief valves in the system, one on the oxidizer tank and one on the fill cart nitrogen line. These pressure relief valves act as a fail-safe in case the pressure in the line or tank was to exceed an expected pressure. The valves will automatically open if the pressure in the line exceeds the set pressure until the line returns below the set pressure. This adds safety to the system since the line will theoretically not reach a pressure over the set pressure on the valve. The relief valve on the nitrogen fill line was set to 2300 psi and the relief valve on the oxidizer tank was set to 2200 psi. The MEOP in both areas was 2000 psi, but the higher set pressure adds a small amount of wiggle

room for the regulator valve to be set higher if future testing determines the need for it due to pressure drops in the system.

4.2. Water Flows

Water flow tests were conducted on various components to characterize the actual flow area at various pressures. Water was used to have a constant density and directly relate the mass flow rate to pressure drop. For these tests, the flow rate was controlled through a cavitating venturi flowmeter. The upstream and downstream pressure were recorded using digital pressure transducers. This process was carried out to get the flow areas of all venturis, orifices, valves, and both sides of the injector. Additionally, spray tests were conducted using water and compressed air through the injector to get a qualitative image of the mixing dynamics. Water was used to represent the oxidizer, and compressed air was used to simulate the low-density, hot fuel as it comes out of the regenerative circuit.

The combustion chamber was water flow tested using the same setup to get a fluid resistance that could be scaled to the fuel coolant during hot fire conditions. Since the fuel coolant density changes as it heats up, the average of the inlet and exit density was used to predict the pressure drop during hot fire. Figure 14 shows the spray tests with water through the central ports and air through the outer ports, as well as the chamber water flow test.

Figure 14. Injector spray visualization (left) and chamber water flow testing (right).

System-level water testing was also done on the test stand with water in both tanks to efficiently examine the performance of nitrogen system before adding nitrous oxide. This

simplified the filling procedure and confirmed that the pressure regulator was giving enough nitrogen flow to keep the tanks pressurized. It also gave a first look at system pressure drops that could be scaled to future tests. These system-level water testing also exposed any issues in the test stand instrumentation, controls, or data acquisition. Throughout water testing multiple valves were giving issues in which they were stuck open, even when the power to them was cut. This is a serious safety risk due to the potential for uncontrolled mixing of combustible propellants. This can lead to a situation where the propellants cannot be cut off from each other, resulting in an uncontrollable combustion process. Because of these inherent safety risks, the problem valves were replaced prior to cold flow testing.

Additionally, a larger than expected pressure drop was found in the system during water flow testing. The tanks were originally pressurized to 1600 psi, but the high mass flow rate through the oxidizer line served for a relatively large pressure drop between the tank and the venturi. To combat this, the decision was made to set the tank pressure to 2000 psi as mentioned in section 3.4. Propellant Tank Design, so that there was a higher pressure of the fuel and oxidizer as it reached the venturi.

4.3. Cold Flows

Cold flow testing was conducted using nitrous oxide on the oxidizer side and water to simulate the fuel. The goal of these tests was to confirm mass flow rates, pressure drops and system-wide functionality at the expected operating pressures and temperatures. No igniters were used in these tests, but electric matches were set off in place of an igniter to verify the mainstage sequence. Another goal from cold flow tests was to get injector arrival times for each propellant. Since the injector orifices were not visible, the injector manifold pressures were used to adjust the valve delays so both propellants would arrive at the same time in future tests. For the fuel, the ethanol arrival time was approximated by scaling the measured water velocity to an ethanol velocity using the different flow rates and densities. This is shown in Equation 4.1 below, which is derived by comparing the two mass flow rates through the same flow area. Since the velocity is inversely proportional to the time it takes to travel through the same feed system, the arrival time can be approximated using Equation 4.2 below.

$$\frac{V_{ethanol}}{V_{H2O}} = \left(\frac{\dot{m}_{ethanol}}{\dot{m}_{H2O}}\right)\left(\frac{\rho_{H2O}}{\rho_{ethanol}}\right) \tag{4.1}$$

$$t_{a,ethanol} = t_{a,H2O}\left(\frac{V_{ethanol}}{V_{H2O}}\right)^{-1} \tag{4.2}$$

4.3.1. Valve Sequencing

The valve sequence that is run during cold flows and hot fires is programmed to line up propellant arrival, control the test duration, and safely shutdown the engine. The sequence

diagram is shown below in Figure 15. The diagram uses timers (T0-T5) to define the interval between events.

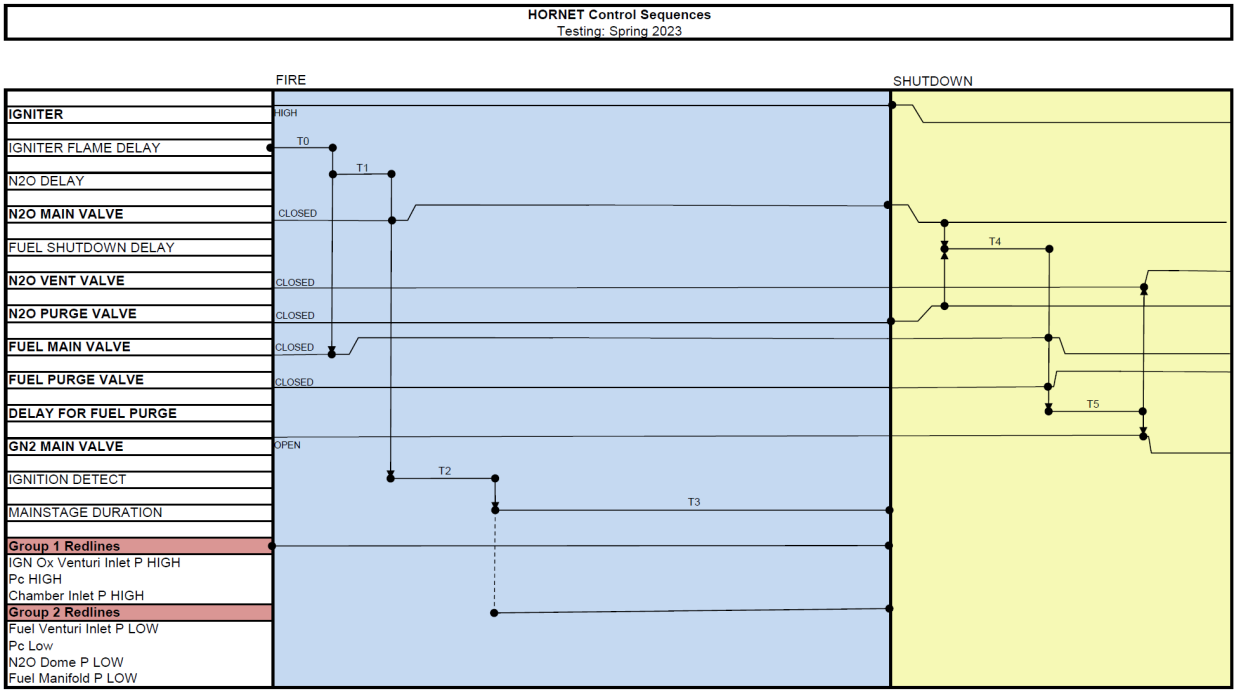

Figure 15. Hot fire control sequence.

The first timer, T0, allows for time for the solid propellant igniter to start fully combusting before propellant starts flowing. T1 defines the time to delay the oxidizer valve to match up arrival time. T2 defines the ignition detect period, where if an increase in chamber pressure is not measured in that interval, then the engine will shut down to avoid pooling propellants in the chamber. Next, T3 defines the targeted mainstage duration and after that begins the shutdown sequence. On shutdown, nitrous oxide is purged first to keep the combustion fuel rich and relatively cooler. Then, after the T4 timer, the fuel is purged to clear it from the feed system and chamber manifolds for the duration of the T5 timer. Following that, all valves are closed except the vent to relieve system pressure. Redlines are separated into two groups, depending on when they were activated. Group 1 redlines are active the entire test duration and group 2 redlines are only activated once ignition is achieved to avoid falsely triggering a redline.

4.4. Hot Fire Tests

After proof testing, water flow and cold flow testing, hot fire tests were conducted to measure the thrust chamber's combustion performance. The key metrics for hot fire testing were chamber pressure, thrust, and coolant temperatures. Additionally, these tests were executed to prove the engine could reliably achieve ignition using solid propellant igniters. Apart from testing logistics and the igniter installation, the hot fire tests were procedurally the same as cold flow testing. GoPro cameras were used to record video at various angles and a FLIR camera was

used to record infrared (IR) video. A black backdrop was used to make the combustion gases more visible. A picture of the fourth hot fire attempt is shown below in Figure 16.

Figure 16. Hot fire test 4.

The test stand was transported to the team's test site in Amherst, OH and procedures and safety checks were followed during setup and testing. See section 7.2. Safety Considerations for the safety precautions put in place for hot fire testing.

5. Test Results

The testing provided data for characterizing the feed system and thrust chamber. All test data was imported and processed in MATLAB, and then additional analysis was done in Excel using steady state values.

5.1. Test Schedule

Table 3 below shows the dates in which the system was tested as well as the achieved chamber pressures, mixture ratios, and durations. The durations shown in the table are defined by the time interval between rise in chamber pressure and when it starts to drop. Water tests and cold flow tests were run during March, with two days of hot fire testing in April. The first day of hot fire testing revealed issues with ignition thought to be caused by a low oxidizer stay time. To fix this, a third lower pressure test was conducted which resulted in about 2.5 seconds of combustion.

Changes to the injector and fuel venturi were made before the second hot fire day, which resulted in two successful high-pressure tests, both at 6 seconds. While the first two hot fire attempts were successful in igniting, the subsequent two attempts later in the day did not ignite. This is outlined further in section 5.2.2. Hot Fire Tests 3-5 Results. For cold flows, the test duration was affected by our oxidizer tank capacity and for hot fires it directly reflects how long we had combustion.

Table 3. Test schedule.

Hornet Test Matrix - Spring 2023					
Test Day	**Test #**	**Pc (psia)**	**MR**	**Duration (sec)**	**Notes**
3/10/2023	CF1	45	2.63	11.69	
3/17/2023	CF2	45	2.63	12.03	
4/2/2023	HF1	45	-	-	Didn't ignite
4/2/2023	HF2	45	-	-	Didn't ignite
4/2/2023	HF3	264	2.15	2.5	Combustion extinguished after 2.5 sec
4/23/2023	HF4	342	5.65	5.67	
4/23/2023	HF5	348	5.55	6.58	
4/23/2023	HF6	45	-	-	Didn't ignite
4/23/2023	HF7	45	-	-	Didn't ignite

5.2. Feed System Pressures

5.2.1. Cold Flows 1 and 2 Results

As mentioned previously, cold flow tests were conducted at our target operating point for hot fire testing to verify the flow rates and pressure drops throughout the system. To generalize our pressure losses between different mass flow rates and densities, a fluid resistance, R, was calculated using Equation 5.1 below. These resistance values are then used to approximate pressure losses for future operating conditions.

$$R = \frac{\Delta P \cdot \rho}{\dot{m}^2} \tag{5.1}$$

The system pressure data from the two cold flows is shown in Figure 17. There was no combustion, but the nitrous oxide generated 45 psig in the chamber as it expanded. An unexpected phenomenon that occurred during the cold flow tests was the oxidizer tank appearing to run out of propellant earlier than predicted. The tank was filled with about 45 lbs. of nitrous oxide (see section 5.6. Nitrous Oxide Filling), which with a flowrate of 2.8 lbm/s should have lasted the full 15 second targeted test duration. However, at ~12 seconds after opening the oxidizer valve, the manifold pressure rose and the chamber pressure dropped, indicating that

there was nitrogen flowing through the system. This was also confirmed visually by the white vapor disappearing at the same time. After all the valves closed, there was still leftover nitrous oxide left in the tank. This phenomenon is thought to be from vortexes forming in the tank as the liquid level drops. The vortexes may have prevented the nitrous oxide from flowing and therefore making it appear as if it had already been depleted.

A second cold flow test was run to see the performance of the pressure-regulating system for a second, full-duration test with lower bottle pressures. The pressure data shows that the tank pressures start at the same pressure as the first cold flow, but over the test duration dropped ~180 psi on the fuel side. This loss was acceptable for a second test, but additional tests would need new nitrogen bottles unless the test durations were shortened.

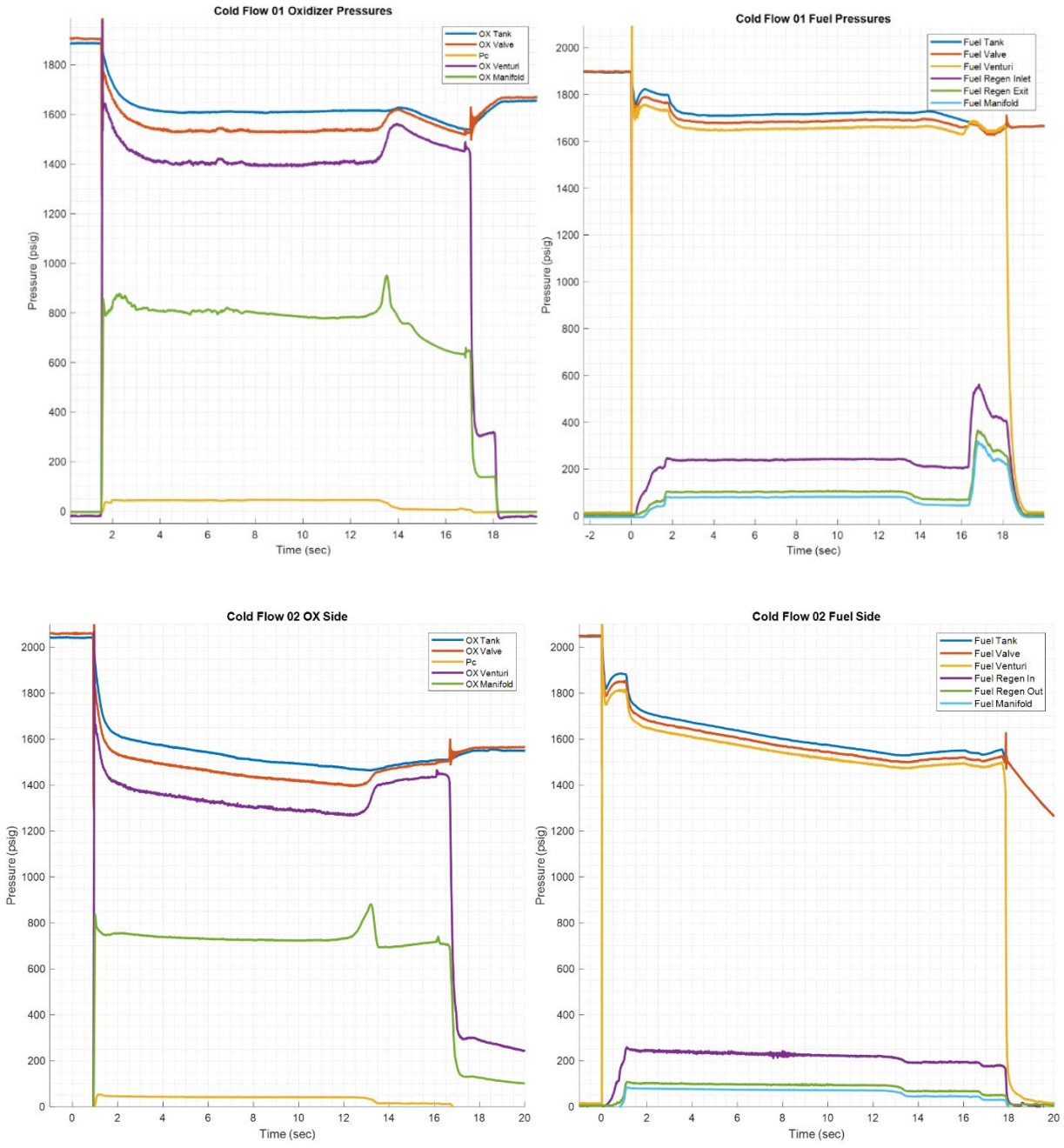

Figure 17. Cold Flow 1 (top) and Cold Flow 2 (bottom) feed system pressures.

5.2.2. Hot Fire Tests 3-5 Results

The pressure data from the three hot fire tests that successfully ignited are shown below in Figures 18-20. Since the first two tests did not ignite, the third hot fire attempt ran at a set pressure of 1000 psig so the pressure could still be regulated despite the nitrogen bottle pressure being low. This can be seen in the reduced pressure in Figure 18 compared to the higher starting pressure of 2000 psi that is seen in Figure 19 and Figure 20. This third test only lasted about 2.5

seconds, and the engine stopped combusting on its own, likely due to its instability, also mentioned in section 5.4.

Due to the ignition and stability problems with hot fire 3, the decision was made to make changes to the oxidizer orifices in the injector and the size of the fuel venturi. The oxidizer orifices were drilled out to lower the pressure drop across the injector, as well as the injection velocity. Additionally, the diameter of the fuel venturi was lowered to allow for a lower mass flow rate and higher MR. The intent was that between less coolant flow rate and hotter combustion, the fuel would lower in density and improve the stiffness. Both changes worked in HF04 and HF05, but because the tests were only ~6 seconds long the chamber never reached thermal steady state.

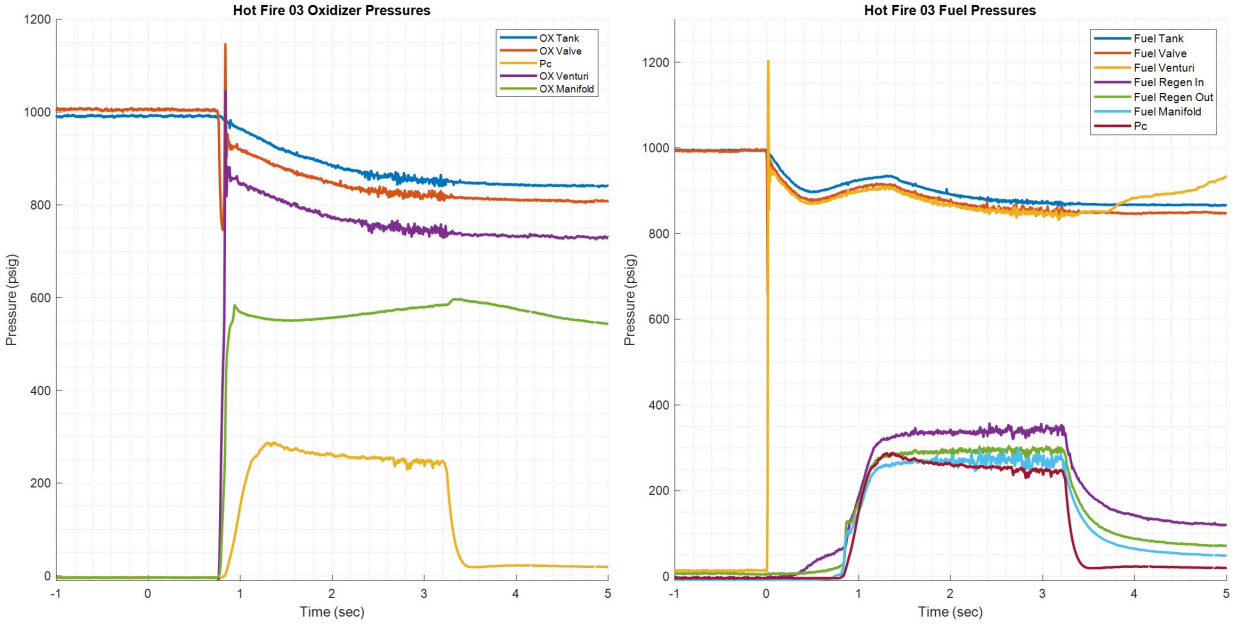

Figure 18. Hot Fire 3 results.

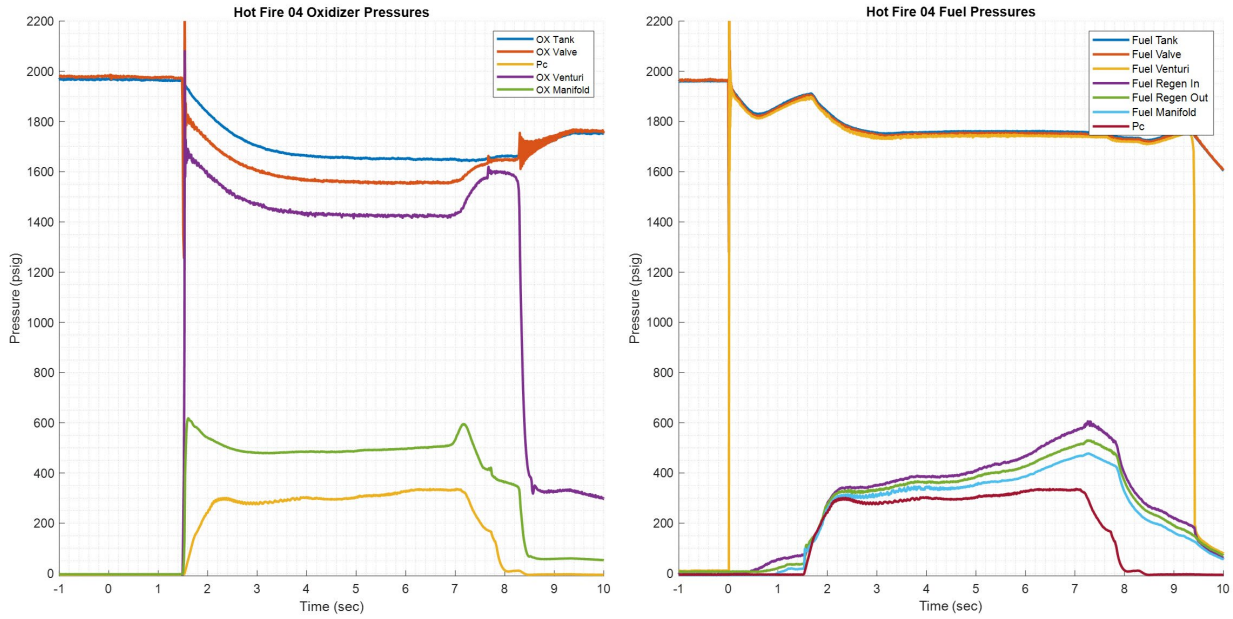

Figure 19. Hot Fire 4 results.

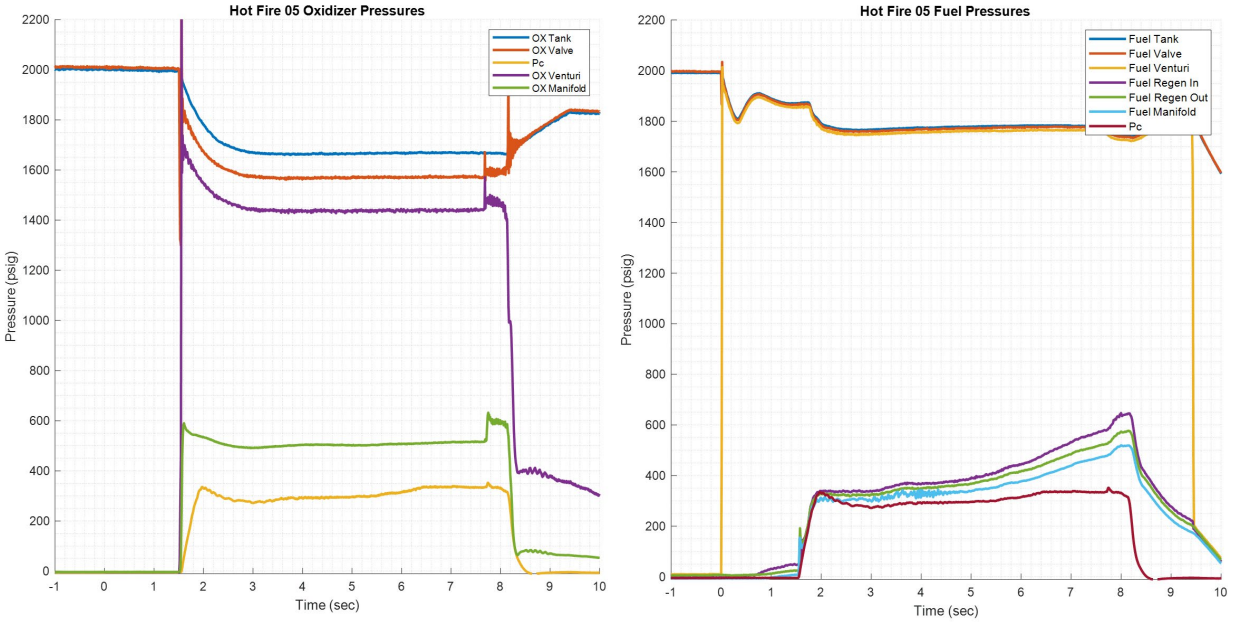

Figure 20. Hot Fire 5 results.

5.3. Flow Rates

The measured propellant flow rates for several of the tests are shown in Table 4 and Table 5 below. The cavitating venturis gave a reliable and easy method to measure mass flow rate. The venturi works by creating a localized, low-pressure area that causes fluids to vaporize and form bubbles, or cavities. These cavities create a repeatable pressure drop that can be used to

accurately measure the mass flow rate of the fluid passing through the venturi. Because these venturis are present in the system, the only way to change the flow rate in a line during testing is by changing the set pressure on the tanks. Given that there is only one pressure regulator, the tank set pressure for the fuel and the oxidizer are coupled and both flow rates will change when the set pressure to the tanks is changed. Having these lines connected is a limiting factor in the design of this engine. This resulted in wasting a lot of the pressure budget in the venturi pressure ratio, which can be seen by the low-pressure ratios across the venturis. The only venturi that wasn't extremely cavitated was the nitrous venturi during HF03. This is because, as mentioned earlier, the tank set pressure was lowered to 1000 psi. A future iteration of the design could achieve the same chamber conditions with a much lower tank pressure by resizing the venturi diameters with the known inlet and downstream pressures.

Table 4. Measured oxidizer mass flow rate calculations.

Test #		Hot Fire 05	Hot Fire 04	Hot Fire 03	Hot Fire 01	Nitrous Cold Flow 01
N2O System		*N2O*	*N2O*	*N2O*	*N2O*	*N2O*
venturi inlet P (psig)		1442.57	1427.22	750.367	1418.23	1402.08
venturi inlet T (deg F)		40.00	36.00	43.40	52.62	52.4
N2O Inj Manifold P (psig)		515.01	496.50	573.63	749.24	812.109
N2O Inj Manifold T (deg F)		40.00	36.00	43.40	48.65	52.4
venturi flow	*Pressure ratio across venturi*	*0.36*	*0.35*	*0.77*	*0.53*	*0.58*
	venturi D_t (in)	**0.160**	**0.160**	**0.160**	**0.160**	**0.160**
	venturi C_d	0.98	0.98	0.98	0.98	0.98
	venturi A_tC_d (in^2)	0.0197	0.0197	0.0197	0.0197	0.0197
	density (lb_m/ft^3) at venturi inlet P & T	58.1	58.7	55.4	56.0	55.9
	saturation pressure (psia)	506.6	479.2	530.9	600.9	599.1
	N2O flow rate (lbm/s)	*3.07*	*3.11*	*1.45*	*2.82*	*2.79*

Table 5. Measured mass fuel flow rate calculations.

Test #		Hot Fire 05	Hot Fire 04	Hot Fire 03	Hot Fire 01	Nitrous Cold Flow 01
Fuel System		*Ethanol*	*Ethanol*	*Ethanol*	*Ethanol*	*H2O*
venturi inlet P (psig)		1763.92	1744.24	847.108	1673.98	1655.76
venturi inlet T (def F)		40	42	58.6	60	50
Fuel Regen Inlet P (psig)		567.761	467.468	336.8	230.771	240.928
Fuel Regen Inlet T (deg F)		94	87	76.8	60	50
venturi flow	*Pressure ratio across venturi*	*0.328*	*0.274*	*0.408*	*0.146*	*0.153*
	venturi D_t (in)	**0.060**	**0.060**	**0.080**	**0.080**	**0.080**
	assumed venturi C_d	0.980	0.980	0.980	0.980	0.980
	venturi A_tC_d (in^2)	0.0028	0.0028	0.0049	0.0049	0.0049
	density (lb_m/ft^3) at venturi inlet P & T	50.7	50.6	49.9	50.1	62.7
	saturation pressure (psia)	0.3	0.3	0.6	0.6	0.2
	Fuel flow rate (lb_m/s)	*0.55*	*0.55*	*0.68*	*0.95*	*1.06*

The load cells underneath the propellant tanks were intended to act as an additional measure of mass flow rate, as well as to measure how much propellant is left in the tank. As shown in Figure 21, the data was able to be smoothed out and around 5-6 seconds into the test the graph becomes very linear. This linear region is where the slope was calculated to find the mass flow rate. It is important to note that for short duration tests, the noise is too high for the load cells to give meaningful data. For the CF01 test, the measured oxidizer flowrate was 2.24 lbm/s and for HF04 it was 2.92 lbm/s. The fuel flow rate was 0.81 lbm/s for CF01 and 0.29 lbm/s for HF04. The variation between the fuel flow rate is due to the difference in venturi used for CF01 and HF04. The venturi diameter was decreased between the two tests, changing the flow rate. When comparing with the values above, the measurements from the load cells are consistently lower than the venturi measurements by 0.19-0.55 lbm/s on the oxidizer side and 0.14-0.26 lbm/s on the fuel side. Some amount of this is likely due to the weight of the nitrogen backfilling, which

for HF04 and HF05 was calculated to be 0.46 lbm/s of nitrogen into the oxidizer tank and 0.09 lbm/s into the fuel tank. Additional error is likely attributed to reaction forces present from propellant line loads.

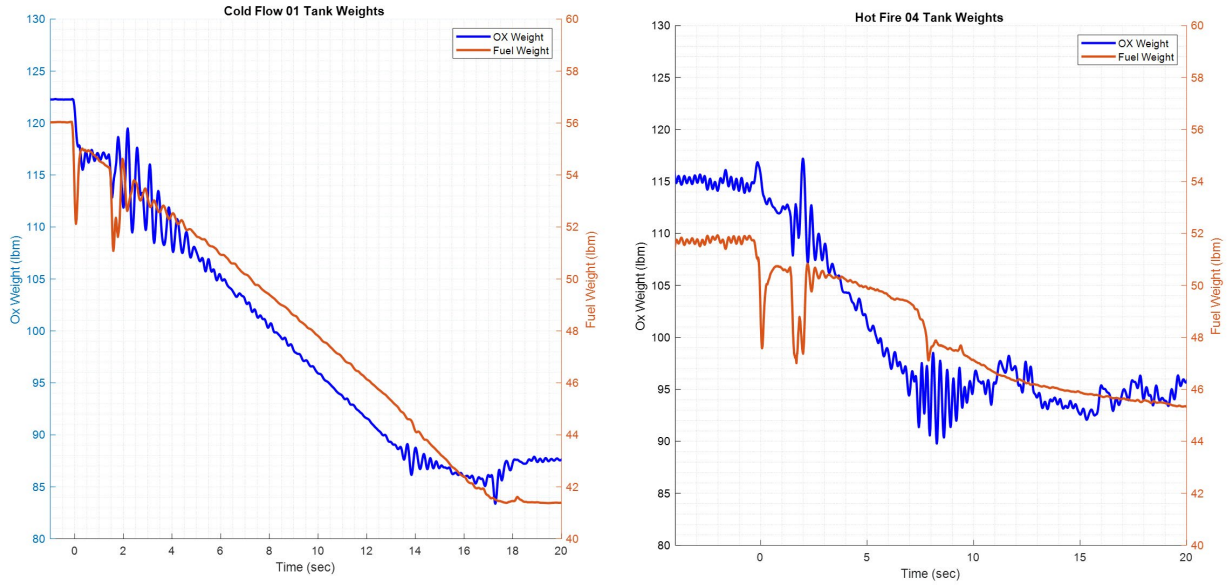

Figure 21. Tank weights during CF1 (left) and HF4 (right)

5.4. Thrust Chamber Performance

The thrust and chamber pressure for each of the three hot fires are shown below in Figure 22. All three tests saw a spike in chamber pressure on startup, which may have been due to issues with startup timing resulting in excess fuel in the chamber. Since the ethanol orifices on the injector printed bigger than expected, the fuel manifold had a low stiffness and the thrust chamber experienced instabilities at 20-30 Hz for HF4 and HF5. The amplitude of the pressure fluctuations was only 2% of the combustion chamber pressure. For HF3, the combustion extinguished after about 2.5 seconds which is thought to be from the instability snuffing out the flame. The ethanol was also expected to lower in density throughout the test, making it more likely to vaporize and increase the injector stiffness, making the combustion more stable, but that did not occur, so the instability never stopped.

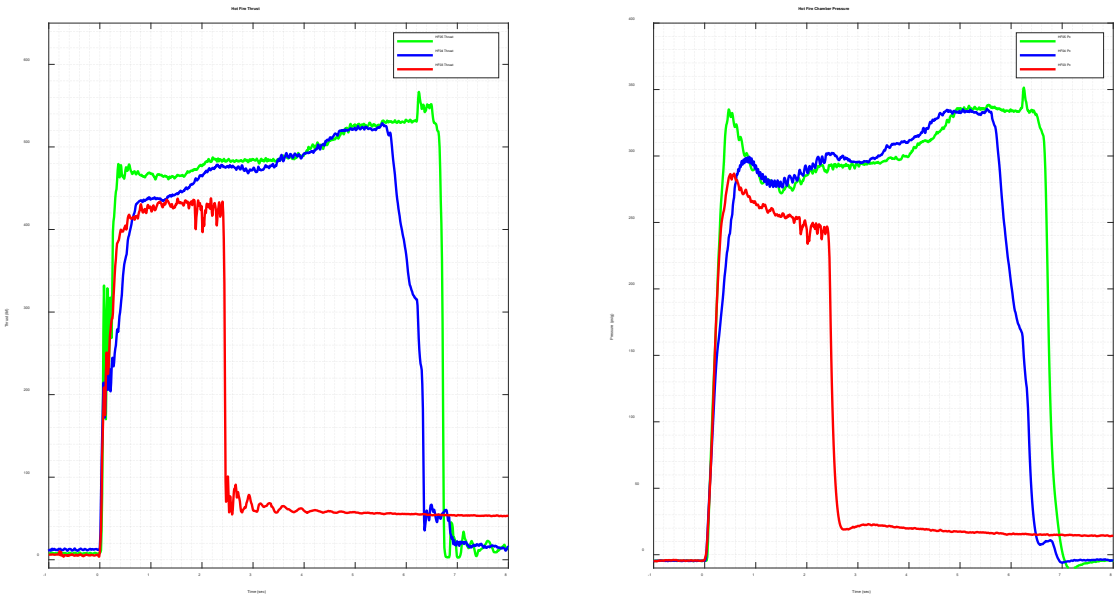

Figure 22. Comparison of hot fire thrust (left) and chamber pressure (right).

Figure 23. Hot fire 5 plume at 2 sec. (left) and 6 sec. (right) after ignition.

For tests 4 and 5, the fuel flow rate was lowered to increase the temperature from the regenerative circuit. As the fuel heated up, the fuel manifold became stiffer and the engine performance improved. This increase in performance can be seen in the chamber pressure and thrust increase for the same mass flow rate. This was also seen visually as the plume became brighter throughout the test, as shown in Figure 23.

5.5. External Pressurant

The nitrogen pressure-regulated system's purpose was to backfill the propellant tank pressures during the test to keep the engine operating at steady state. One consideration that

wasn't accounted for initially was the pressure losses from the nitrogen flowing through the system. There was a pressure drop through the regulator that lowered the regulator exit pressure by ~200 psi. Additionally, because of the different mass flow rates of nitrogen required for the fuel and oxidizer tank, the regulated pressure in each tank would be different, and can be seen in Figure 24.

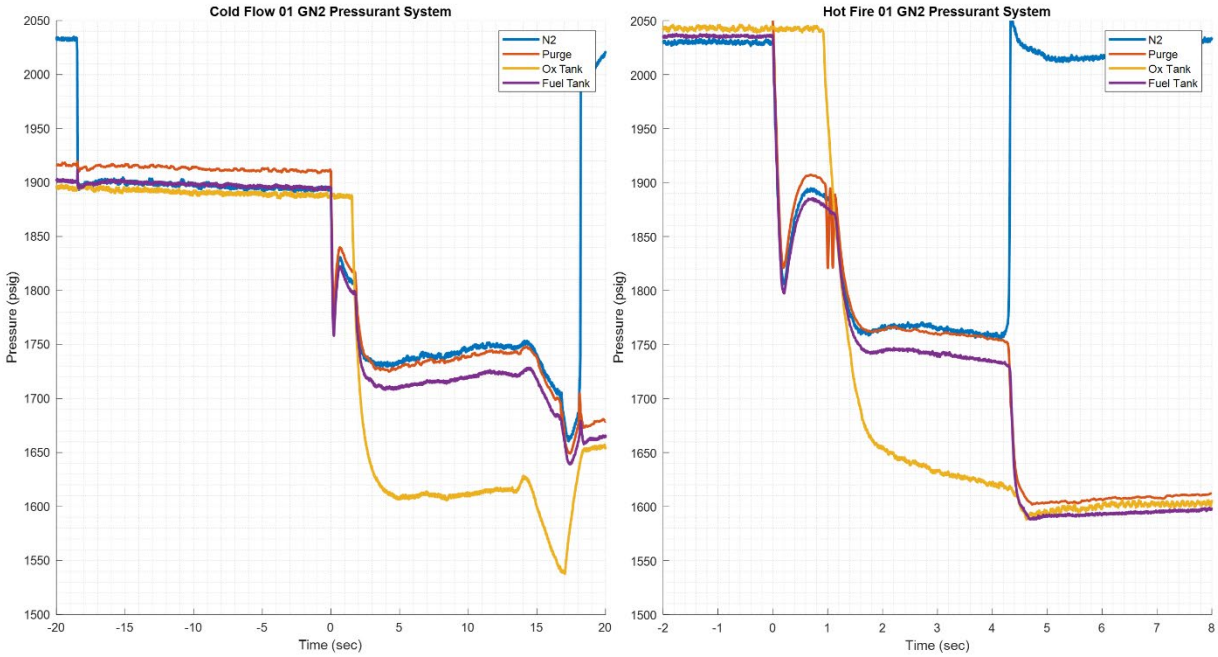

Figure 24. Graphs from the GN2 pressurant system during a cold flow and hot fire.

5.6. Nitrous Oxide Filling

As mentioned in section 3.4.1. Filling and Draining Procedures, the nitrous oxide fill valve is closed periodically throughout the fill procedure to allow for the oxidizer tank to vent off excess vapor pressure and create a larger difference in pressure from the nitrous oxide cylinder to the tank. This can be seen in Figure 25 as the tank pressure and weight increase in bursts from the opening and closing of the nitrous oxide fill valve.

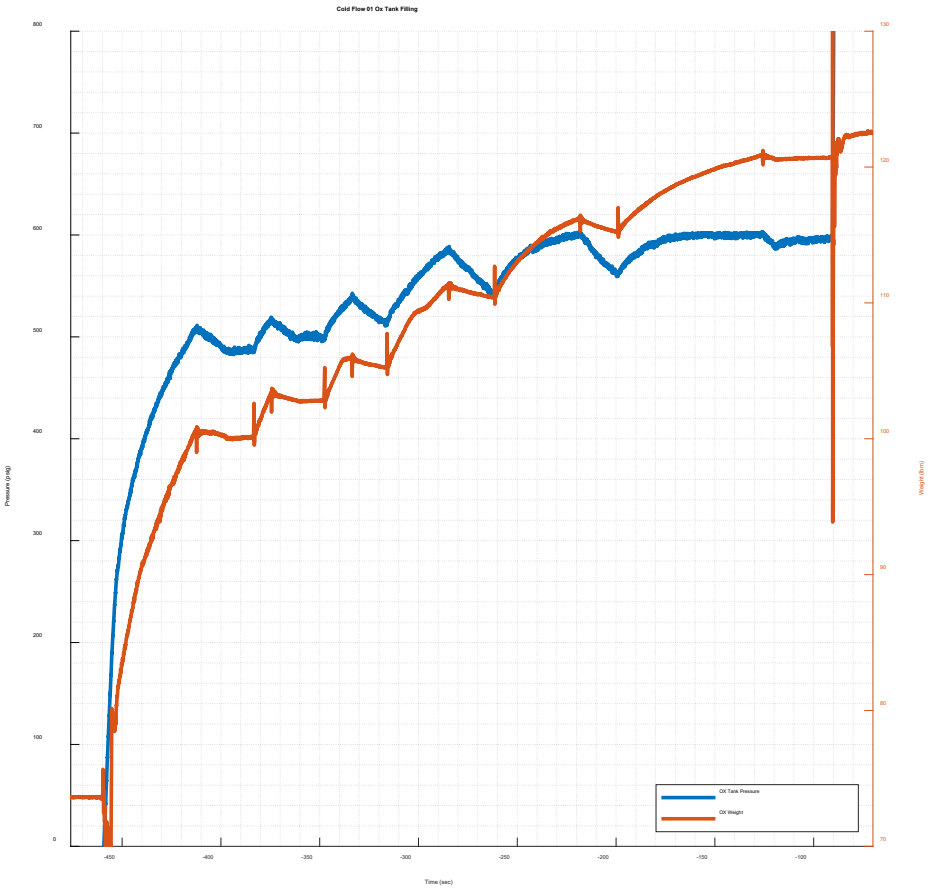

Figure 25. Ox tank pressure and weight during the fill procedure from cold flow 1.

5.7. Ignition Discussion

As mentioned previously, 4 out of 7 hot fire attempts did not properly ignite. It is thought that the higher mass flow rates and more dense nitrous oxide injection made it more difficult to ignite the engine. The igniter used in hot fires 1 and 2 is the same igniter that was used in the hot fire testing done by the Akronauts with previous engines, as mentioned in section 2.5. Igniter. Hot fire 1 had the igniter taped to the chamber, and the second attempt utilized a 3D printed igniter holder, however neither attempt properly ignited the engine. After the igniter holder failed to fix the ignition issue, it was speculated that there was a problem with the way the igniter burned. It was thought that the propellants started snuffing the igniter as soon as they entered the chamber because most of the sparks from the igniter were moving toward the injector, not the combustion chamber wall. To fix this problem, the igniter was modified to have the front and back ends capped, with only four holes open for sparks on the curved face of the igniter, as seen in the right image in Figure 7. This way the sparks were theoretically not snuffed by the propellants and could properly ignite the engine. The modified igniter was used on hot fire attempt 3 and successful ignition was achieved.

This modified igniter was also used for hot fire attempts 4 through 7. As mentioned in 5.2.2. Hot Fire Tests 3-5 Results, ignition was achieved after changing the fuel venturi and the oxidizer orifices, but the timings in which the fuel and oxidizer arrived at the injector were slightly modified as well. The fuel timing was changed in an attempt to have the fuel and oxidizer reach the engine at roughly the same time. There ended up being a slight fuel lead, even with the modified flow rates, as the fuel reached the injector about a half of a second before the oxidizer. Regardless, the engine still achieved proper ignition for the 4^{th} and 5^{th} hot fire attempt.

6. Costs

All costs for the project are outlined below. The costs are divided between donated parts, the propellants used, and purchased items.

6.1. Donated Parts

The following is a table of the parts used in the test stand and the cost of the engine itself. All the parts in Table 6 have been donated to the project. Most components were used in the feed system and external pressurant and purge system.

Table 6. Complete list of donated components and monetary equivalent value.

Part Description	Vendor	Price per Pkg.	# Pkgs.	Total
SS In-Line Particulate Filter, 3/8" Tube Fitting, 60 Micro	Swagelok	$ 121.26	2.00	$ 242.52
*3/8" ABVA W PNEUMATIC ACTUATOR (N/C) & 12V S(	Swagelok	$ 806.03	1.00	$ 806.03
SS 60 Series Ball Valve, Reinforced PTFE Seats, 3/8" FN	Swagelok	$ 240.94	2.00	$ 481.88
SS 40G Series Ball Valve, 1.6 Cv, 1/4" MNPT x 1/4" Tub	Swagelok	$ 108.01	1.00	$ 108.01
SS High Pressure Proportional Relief Valve, 1/4" MNPT	Swagelok	$ 178.72	3.00	$ 536.16
Purple Spring Kit for R3A Series Proportional Relief Val	Swagelok	$ 4.98	3.00	$ 14.94
Orange Spring Kit for R3A Series Proportional Relief Va	Swagelok	$ 4.98	3.00	$ 14.94
Brown Spring Kit for R3A Series Proportional Relief Val	Swagelok	$ 4.98	2.00	$ 9.96
SS Poppet 6000 psig (413 bar) Check Valve, 1/4" Tube F	Swagelok	$ 68.37	2.00	$ 136.74
SS Poppet 6000 psig (413 bar) Check Valve, 3/8" Tube F	Swagelok	$ 102.61	1.00	$ 102.61
SPECIAL: RPHS REGULATOR	Swagelok	$ 1,794.64	1.00	$ 1,794.64
SPECIAL: 316 SS, Pressure Gauge, 63C Model, 2-1/2" D	Swagelok	$ 68.33	1.00	$ 68.33
SS Tube Fitting, Male Connector, 3/8" Tube OD x 3/8"	Swagelok	$ 13.57	10.00	$ 135.70
SS Tube Fitting, Male Connector, 1/4" Tube OD x 1/4"	Swagelok	$ 8.80	10.00	$ 88.00
SS Tube Fitting, Male Tube Adapter, 1/4" Tube OD x 3/	Swagelok	$ 9.75	10.00	$ 97.50
SS Tube Fitting, Female Connector, 1/4" Tube OD x 1/4	Swagelok	$ 14.31	3.00	$ 42.93
SS Pipe Fitting, Cross, 3/8" FNPT	Swagelok	$ 72.19	5.00	$ 360.95
SS Tube Fitting, Union, 3/8" Tube OD	Swagelok	$ 19.40	5.00	$ 97.00
SS Tube Fitting, Union, 1/4" Tube OD	Swagelok	$ 13.67	5.00	$ 68.35
316 SS Ferrule Set (1 Front Ferrule/1 Back Ferrule) for	Swagelok	$ 2.92	5.00	$ 14.60
316 SS Ferrule Set (1 Front Ferrule/1 Back Ferrule) for	Swagelok	$ 2.34	5.00	$ 11.70
316 SS Cap for 1/4" OD Tubing	Swagelok	$ 6.89	8.00	$ 55.12
316 SS Cap for 3/8" OD Tubing	Swagelok	$ 9.33	6.00	$ 55.98
316 SS Cap for 1/2" OD Tubing	Swagelok	$ 13.89	1.00	$ 13.89
SS Tube Fitting, Female Tube Adapter, 1/8" Tube OD x	Swagelok	$ 18.76	10.00	$ 187.60
LC103B-1K STAINLESS STEEL S-BEAM LOAD CELL, 1K	Omega	$ 243.99	2.00	$ 487.98
C103B-200 STAINLESS STEEL S-BEAM LOAD CELL,	Omega	$ 243.99	2.00	$ 487.98
G2S07NQ9GMA TURBINE FLOWMETER,TOTAL, RATE	Omega	$ 875.00	2.00	$ 1,750.00
PX119-5KGI 5000 PSIG CURRENT PRES TRAN	Omega	$ 116.31	8.00	$ 930.48
PX309-2KGI 2000 PSIG CURRENT PRES TRAN	Omega	$ 331.43	3.00	$ 994.29
EQIN-18G-12 QD T/C WITH MOLDED CONNECTOR	Omega	$ 45.58	5.00	$ 227.90
KQXL-18G-12 QD T/C WITH MOLDED CONNECTOR	Omega	$ 47.56	15.00	$ 713.40
ETM-375M-500BARA (Pressure Transducer, 7250 psi)	Kulite	$ 1,144.00	1.00	$ 1,144.00
ETM-375M-210BARA (Pressure Transducer, 3050 psi)	Kulite	$ 1,144.00	1.00	$ 1,144.00
ETM-HT-375MCO-70BARA (5V DC Pressure Transduce	Kulite	$ 1,553.00	2.00	$ 3,106.00
HiP eTensifier Pump Model 100	HiP	$ 3,155.30	1.00	$ 3,155.30
SCE-36N2406LP Nema-1 Enclosure	Saginaw	$ 218.64	1.00	$ 218.64
SCE-36N24MP Nema-1 Subpanel	Saginaw	$ 59.85	1.00	$ 59.85
12-feet of 6061 Al 6" OD 5.5" ID	MK Morse	$ 900.00	1.00	$ 900.00
HORNET Engine Manufacturing and Post Processing	NASA	$ 18,000.00	1.00	$ 18,000.00
TOTAL			148	$ 38,865.900

6.2. Propellant

Two main companies were considered when purchasing propellant, AirGas and Summit Racing. Summit Racing was used for previous nitrous oxide purchases by the Akronauts Design team, but their volume of nitrous oxide cylinders was too low. Due to this, AirGas was the vendor of choice to supply the nitrous oxide and nitrogen cylinders for testing. Ethanol was purchased from The University of Akron Chemical Stores through the Department of Mechanical Engineering. The propellant costs for the project are listed in Table 7; shipping is included in the totals for each type of propellant.

Table 7. Propellant costs.

Propellant Costs		
Nitrous Oxide		
# of Bottles Purchased		6
Total Spent on Nitrous	$	2,228.61
Nitrogen		
# of Bottles Purchased		11
Total Spent on Nitrogen	$	845.32
Ethanol		
# of Gallons Purchased		10
Total Spent on Ethanol	$	103.40
Total Spent on Propellants	$	3,177.33

6.3 Purchased Items

Even though plenty of equipment and components were donated to the project, multiple items needed to be purchased. Most things were purchased through the Akronauts Design Team and the budget was shared through them. A few companies gave a discount on their products, the most notable being LabJack, who gave a 50% off discount to purchase DAQs for the project. An exhaustive list of purchases for the project is outlined in Table 8. The valves were a high cost due to the valve change post-waterflow testing.

Table 8. Purchased items.

Purchased Items		
Item	**Cost**	
Tubing, multiple diam	$	398.45
Fittings/Gauges	$	2,115.38
Hardware	$	1,014.28
Electronics	$	2,343.06
LabJack DAQs	$	322.54
Tools	$	298.62
Valves	$	4,438.57

7. Conclusion

A regeneratively cooled liquid rocket engine was successfully designed, manufactured, and tested throughout the course of the 2022-2023 school year. The authors and students on the Akronauts who worked on this project have gained significant knowledge and hands-on experience in the liquid propulsion industry through this project. Three successful hot fire tests

were completed and the Akronauts Design Team was able to test their first AM, regeneratively cooled liquid rocket engine.

7.1. Accomplishments

The main goal of the project was to update the infrastructure and liquid engine test stand at the University of Akron, along with expanding the Akronauts' propulsion capabilities. The objective was to successfully design, manufacture, build, and test a regeneratively cooled liquid rocket engine and the supporting feed system for a 15 second hot fire. Despite the 15 second hot fire not being successfully completed, the engine underwent comprehensive design, manufacturing, and testing processes, which enabled it to be accurately characterized. The engine's ability to produce hot fire test data that aligns closely with expected values is a notable accomplishment, especially given the challenges encountered during the testing process. Despite numerous unexpected challenges that arose during the project, causing interim timelines to be postponed, the authors and Akronauts Design Team ultimately succeeded in achieving their original objective of conducting a hot fire test during the first weekend of April. Furthermore, the team was able to refine the system based on their earlier results, and subsequently retested it at the same site three weeks later.

A working feed system was successfully designed and built for the engine, with working controls and data acquisition in various locations on the feed system to quantify the performance of the engine. Water blowdowns, cold flows, and hot fires were all successfully completed. The lessons learned along the way gave great insight into how the system operated, and the changes made to the system with each testing iteration gave an anticipated change to the results. Much was learned about fluids, thermodynamics, liquid rocket engines, and more throughout the completion of this project. The test stand infrastructure for the Akronauts Design Team was successfully upgraded and will be used in future years to expand the capabilities of the design team.

7.2. Uncertainties

The team was fortunate to have been able to have so many quality sensors and valves donated to this project. The quality parts and high sample rate help to reduce the uncertainties in the data analysis. Testing also helped to bring any issues to light, whether it be mechanical issues or the software reading a voltage incorrectly. These were all fixed prior to the hot fire tests, and it is believed that the data received from any hot fire tests is accurate to what happened in the system.

However, there were a few uncertainties that surfaced post-testing. The third hot fire that was completed only lasted about 2.5 seconds. There was enough propellant for it to have gone on longer, but the engine stopped combusting by itself. It is believed that the engine chugged and became so unstable that it stopped combusting. As mentioned in section 5.4. Thrust Chamber Performance, the combustion also started out with the pressure in the chamber being higher than

the pressure in the fuel manifold. Theoretically this would be enough to stop combustion because the flow direction would be backwards, but the combustion kept going and the fuel manifold pressure got to a higher pressure than the chamber shortly after. The combustion stopped after this. It was speculated that the chamber pressure was still higher than the fuel manifold pressure and it wasn't as apparent on the graphs due to the smoothing of the data. The pressures were so close that it is possible it was still chugging and the low difference in manifold to chamber pressure is what stopped the engine from combusting. It is still not known for certain. An image of the shutdown can be seen in Figure 26, with a fireball of the last bit of burned propellant shown on the lefthand side of the image.

Figure 26. Image showing the engine shutdown after the third hot fire.

7.2. Safety Considerations

There was a large focus on safety throughout the project. When the project started, the team already had a good relationship with the University's Environmental Health and Safety Department that approved the testing operations at the University and the NOTRA test site. As mentioned before, hydrostatic proof testing was done on all systems to verify they were rated above the expected pressure.

Another safety consideration was the safety blast radius for hot fire testing. For this, the Federal Aviation Administration's guide for Calculation of Safety Clear Zones was referenced [14]. For the analysis, our propellants were conservatively assumed to be liquid oxygen and RP-1 since nitrous oxide and ethanol were not listed. The total propellant weight upon testing was about 60 lbs. Using this, the net explosive weight (*NEW*) was calculated using Equation 7.1 below with a yield factor of 0.1 for static test stands.

$$NEW = 0.1 \times 60\ lbs = 6\ lbs \tag{7.1}$$

Then, the peak incident overpressure distance, *D,* and hazardous fragmentation distance (*HFD*) were calculated using Equations 7.2 and 7.3 below. The overpressure distance is the distance from the explosion that a shockwave of 1.0 psi will travel. The hazardous fragmentation

distance is the distance from the point of explosion to the point where fragments generated by the explosion are no longer dangerous to people in the open. Note that Equation 7.3 only applies to net explosive weights less than 100 lbs. It was calculated that the overpressure distance and hazardous fragmentation distance were 90 ft and 433 ft, respectively. To follow this, the control room trailer was placed 450 ft away from the test stand for hot fire testing.

$$D = 45 \cdot (NEW)^{\frac{1}{3}} \tag{7.2}$$

$$HFD = 291.3 + [79.2 \cdot \ln(NEW)] \tag{7.3}$$

Additionally, finite element analysis (FEA) was conducted on various critical parts such as the engine mounting plate and thrust support to ensure they could withstand the expected loads. The steel thrust support was analyzed at a theoretical maximum load of 2000 lbf and at that force had a factor of safety of 2.15. Additionally, the thrust support would see a maximum deflection less than 0.002 in. The Al 6061 mounting plate had a factor of safety of 2.4 at a 2000 lbf load and deflected 0.0018 in.

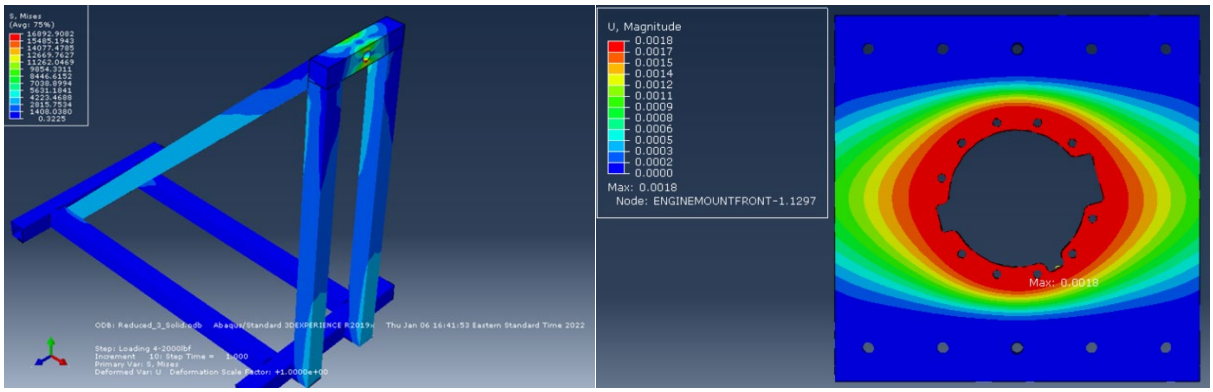

Figure 27. Thrust support stress (left) and engine mounting plate deflection (right).

Lastly, procedures for all testing operations were written for testing and practiced through water flows before using propellant. The procedures ensured that nobody was near the stand when it was pressurized or filled with nitrous oxide. A technical readiness review (TRR) was conducted with the team and mentors from industry prior to testing with propellants.

7.3. Ethical Considerations

There are many things that can be ethically considered when dealing with liquid rocket engines or additive manufacturing, some of the most notable being safety and environmental impact. The safety concerns surrounding this project are outlined in the section above, but it is of course important for the safety of humans to come into consideration regarding testing of any kind. The project was completed in a way that minimizes risk to people and the environment. Industry and on-campus advisors were involved in multiple decisions along the way, and the safety of individuals came first throughout the entire design, build, and test process.

There are a few chemical byproducts from the combustion of nitrous oxide and ethanol, including water vapor (H2O), carbon dioxide (CO2), nitrogen (N2), and trace amounts of nitrogen oxides (NOx) and carbon monoxide (CO). According to a NASA Environmental Impact Assessment (EIA) regarding the environmental impact due to rocket engine combustion, the maximum carbon monoxide concentration level is 0.00255 mg/m^3 [15]. Along with this, the national primary ambient air quality standard should not exceed 40 mg/m^3 for a 1-hour concentration [15]. Due to the actual tests being only 6-seconds, the total amount of CO being created from the combustion reaction is very little and is lower than the ambient air quality standards.

7.4. Future Work

This project was very successful in learning how to design and test a regeneratively cooled liquid rocket engine. Additionally, it built up the feed system on the Akronauts Design Team's test stand that can be used for testing future TCAs. Moving forward, the team will start development towards integrating the engine into a flight vehicle. In this context, there are several improvements that can be made. First, by using test data the engine's operating point could be changed to a higher chamber pressure, resulting in more thrust and higher nozzle efficiency. Additionally, the injector may need to be redesigned to have a higher stiffness on startup. A more reliable ignition method will be needed, which might involve an augmented spark igniter being integrated into the injector. The venturis should be resized to manage the pressure budget of the system more efficiently. A burn time will need be selected that makes sense for the flight vehicle's thrust to weight ratio and target altitude.

Acknowledgments

The completion of this project was only possible because of the immense support received from our industry sponsors, mentors, and the Akronauts Rocket Design Team. The authors would first like to thank the profound support from this project's industry sponsors: Swagelok, OMEGA, Kulite, High Pressure Equipment, Saginaw Controls, LabJack, MK Morse, and Flow Systems.

The authors would also like to thank NASA Marshall Space Flight Center, ER13, the machinists in ET10, and the Pathways Office for their help in printing and post processing the test article for this work as part of the Pathways Intern program experience, but most notably Thomas Teasley from NASA MSFC for his help and mentorship throughout this project.

The authors are very grateful for the University of Akron's College of Engineering and William's Honors College, who financially sponsored this senior design project through their support of the Akronauts Design Team. Finally, the authors would like to thank the Akronauts Design Team members that helped in the design, building, and troubleshooting of the feed system and controls systems, most especially Ana Clecia Alves Almeida, Aaron Hoffman, and Josh Slivka. Their support along this journey helped make the experience a memorable one.

References

[1] Gradl, P., Mireles, O., and Andrews, N. *Introduction to Additive Manufacturing for Propulsion and Energy Systems*. 2021.

[2] Blakey-Milner, B., Gradl, P., Snedden, G., Brooks, M., Pitot, J., Lopez, E., Leary, M., Berto, F., and du Plessis, A. "Metal Additive Manufacturing in Aerospace: A Review." *Materials and Design*, Vol. 209, 2021. https://doi.org/10.1016/j.matdes.2021.110008.

[3] Hunter, L. W., Brackett, D., Brierley, N., Yang, J., and Attallah, M. M. "Assessment of Trapped Powder Removal and Inspection Strategies for Powder Bed Fusion Techniques." *International Journal of Advanced Manufacturing Technology*, Vol. 106, Nos. 9–10, 2020, pp. 4521–4532. https://doi.org/10.1007/s00170-020-04930-w.

[4] Gradl, P. R., Protz, C., Cooper, K., Garcia, C., Ellis, D., and Evans, L. "GRCop-42 Development and Hot-Fire Testing Using Additive Manufacturing Powder Bed Fusion for Channel-Cooled Combustion Chambers." *55th AIAA/SAE/ASEE Joint Propulsion Conference*, 2019. https://doi.org/10.2514/6.2019-4228.

[5] Huzel, D. K., and Liang, D. H. H. *DESIGN OF LIQUID PROPELLANT ROCKET ENGINES NASA SP-125*. 1967.

[6] Sutton, G. P., and Biblarz, O. *Rocket Propulsion Elements*. John Wiley & Sons, Inc., Hoboken, New Jersey., 2017.

[7] Anderson, J. D. *Modern Compressible Flow*. 2003.

[8] Waxman, B. S., Zimmerman, J. E., Cantwell, B. J., Zilliac, G. G., and Wells, E. C. *Mass Flow Rate and Isolation Characteristics of Injectors for Use with Self-Pressurizing Oxidizers in Hybrid Rockets*. 2013.

[9] Ghassemi, H., and Fasih, H. F. "Application of Small Size Cavitating Venturi as Flow Controller and Flow Meter." *Flow Measurement and Instrumentation*, Vol. 22, No. 5, 2011, pp. 406–412. https://doi.org/10.1016/J.FLOWMEASINST.2011.05.001.

[10] Zhang, T., Liu, L., Guo, Q., Chen, Z., and Hu, S. "Flow of Nitrous Oxide in a Venturi Tube under Conditions of a Hybrid Rocket Motor." *FirePhysChem*, Vol. 1, No. 4, 2021, pp. 199–204. https://doi.org/10.1016/j.fpc.2021.11.008.

[11] Liu, X., Lao, L., and Falcone, G. "A Comprehensive Assessment of Correlations for Two-Phase Flow through Venturi Tubes." *Journal of Natural Gas Science and Engineering*, Vol. 78, 2020. https://doi.org/10.1016/j.jngse.2020.103323.

[12] Newlands, R. *The Physics of Nitrous Oxide*.

[13] Sennott, A., and Sharp, C. *How to Design Pressure Vessels, Propellant Tanks, and Rocket Motor Casings*.

[14] Federal Aviation Administration. *Guide 437.53-1 Calculation of Safety Clear Zones for Experimental Permits under 14 CFR § 437.53(a)*. 2011.

[15] John C. Stennis Space Center. "Component and Subsystem Development Test Facility Environmental Assessment March 1989."

Appendix A Codes and Standards Used

The following is a table showing the codes and standards complied to for the design of the engine and test stand, along with the instruments and design constraints that comply to the applicable code or standard.

Code/Standard Name	Applications that Comply
ISO 376: Load Cell Calibration Standard	200-lb Omega Load Cell
NASA-STD-6030: Additive Manufacturing Requirements for Spaceflight Systems	Injector and Combustion Chamber
NASA-STD-8719.17: NASA Requirements for Ground-Based Pressure Vessels and Pressurized Systems (PVS)	Propellant Tanks and Feed System
ASTM F2362-03(2019): Standard Specification for Temperature Monitoring Equipment	E-type and K-type Thermocouples
ASME PTC 19.2: Pressure Measurement Instruments and Apparatus Supplement	Pressure Transducers
MSFC-SPEC-3717: SPECIFICATION FOR CONTROL AND QUALIFICATION OF LASER POWDER BED FUSION METALLURGICAL PROCESSES	Engine Powder Bed Fusion Manufacturing